Bounds on top operators in the SMEFT from entanglement measurements

Work in progress

Pablo Copete Garrido (MSc), Fernando Cornet-Gómez, Belén Durán González (MSc), Federica Fabbri, Víctor Miralles, Marcos Miralles López, **María Moreno Llácer*** and Marcel Vos,
***IFIC (Uni. Valencia and CSIC), Spain**

Quantum tests in collider physics, Merton College, Oxford, October 2024

- Both ATLAS and CMS have observed quantum entanglement in events with top quark pairs.

- These new measurements can be included in global fits to constrain the top-quark related Wilson coeficients of the Standard Model Effective Field Theory (SMEFT).

→ Talk divided into two parts:

- Understanding parton-to-detector level migration effects

- SMEFT bounds from recent entanglement measurements

From CERN EP seminar, Giulia Negro (CMS)

Entanglement of top quarks

- Can be measured using **spin correlations variables**
- Depends on production mode, $m_{t\bar{t}}$, scattering angle of the top quark (Θ)
- SM predicts entangled states:
  - at the **production threshold region** in gg fusion production
  - at the **boosted region for central production** of the $t\bar{t}$ system

high relative velocity of top quarks
→ space-like separated events

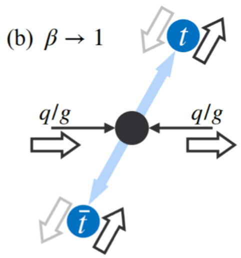

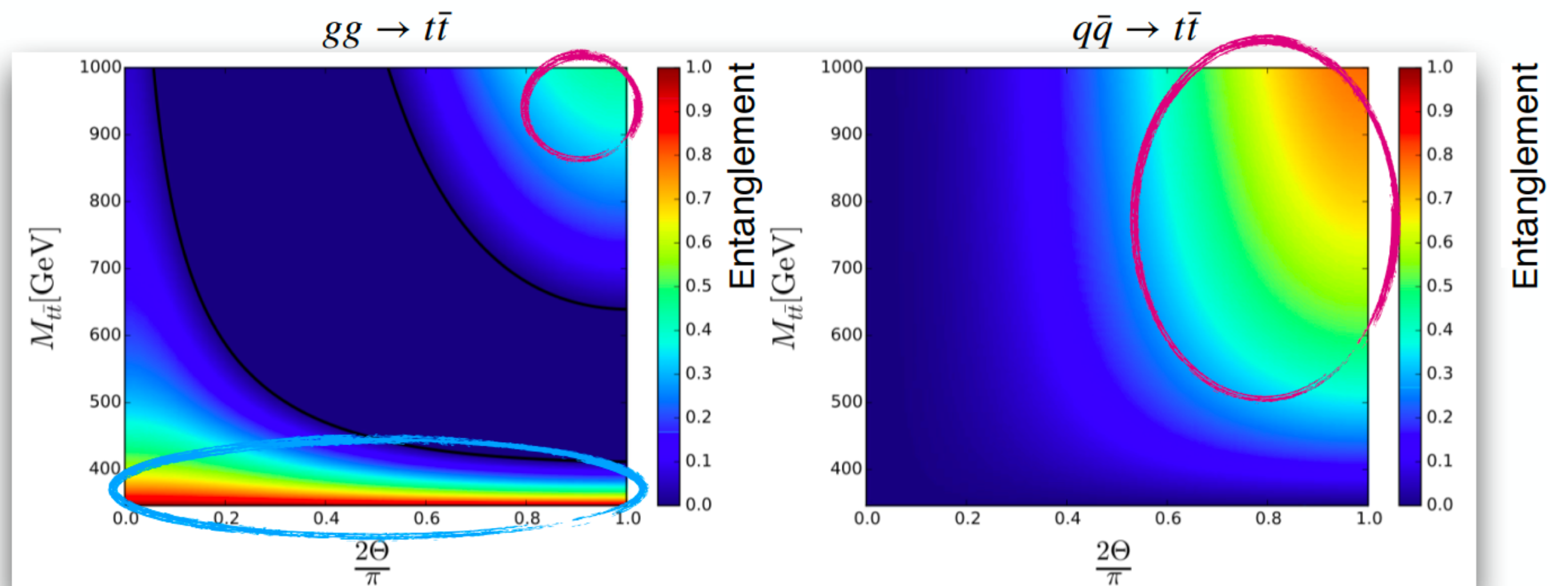

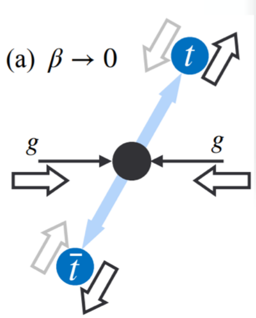

low relative velocity of top quarks
→ time-like separated events

Afik, De Nova
[Eur. Phys. J. Plus **136**, 907]

From CERN EP seminar, Giulia Negro (CMS)

How to probe entanglement

- Four maximally entangled states: $|\Phi^{\pm}\rangle = \frac{1}{\sqrt{2}}\left(|\uparrow\uparrow\rangle \pm |\downarrow\downarrow\rangle\right)$

$$|\Psi^{\pm}\rangle = \frac{1}{\sqrt{2}}\left(|\uparrow\downarrow\rangle \pm |\downarrow\uparrow\rangle\right)$$

Afik, De Nova
Eur. Phys. J. Plus **136**, 907

$gg \to t\bar{t}$

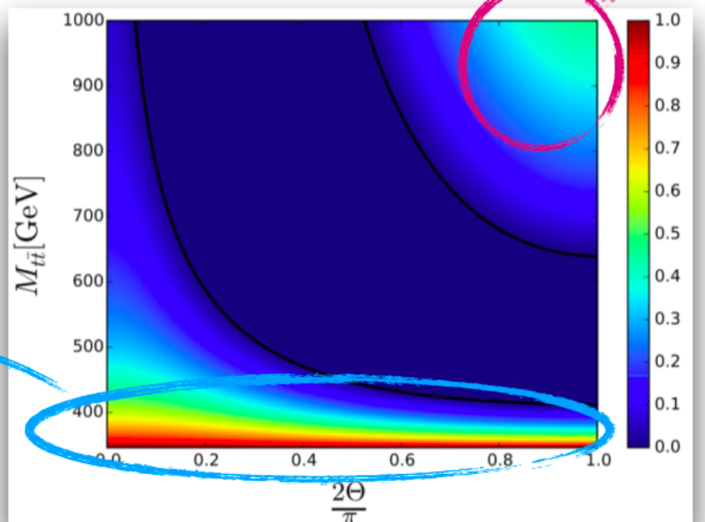

- Spin-triplet vector state ($\Phi^+ - \Phi^-$, Ψ^+, $\Phi^+ + \Phi^-$)
- At high $m_{t\bar{t}}$ and low $|\cos\Theta|$: $C_{kk} < 0$ and $C_{rr} < 0$

$$\Delta_E = C_{nn} - C_{rr} - C_{kk} = 3\tilde{D} > 1$$

$$\to \tilde{D} > 1/3$$

- Spin-singlet pseudoscalar state Ψ^-
- At low $m_{t\bar{t}}$: $C_{rr} > 0$ and $C_{kk} > 0$

$$\Delta_E = C_{nn} + C_{rr} + C_{kk} = Tr[C] = -3D > 1$$

$$D = -\frac{\mathrm{tr}[C]}{3} \to D < -1/3$$

$$\Delta_E = C_{nn} + |C_{rr} + C_{kk}| > 1$$

Sufficient condition for entanglement

→ **measure D, $\tilde{D}$ to access entanglement information in top quark events!**

Sensitive observables to entanglement with top quarks

Sketch from PRD 100 (2019) 072002

Helicity basis $\{\hat{k}, \hat{r}, \hat{n}\}$

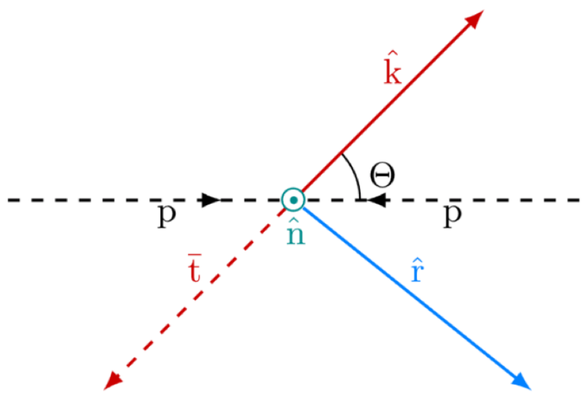

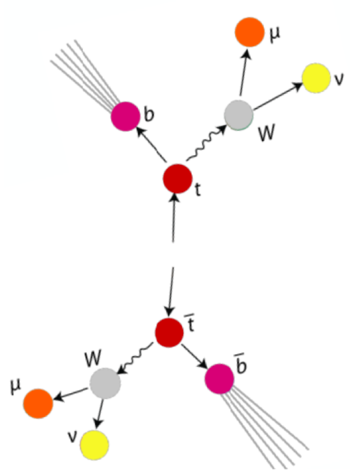

Threshold
$$\frac{1}{\sigma}\frac{d\sigma}{d\cos\theta_{ab}} = \frac{1}{2}\left(1 + \alpha_a\alpha_b D\cos\theta_{ab}\right)$$

being $\cos\theta_{ab} \equiv \hat{p}_a \cdot \hat{p}_b$

angle between the directions of two decay products measured in their parent top quark and antiquark rest frames

Boosted
$$\frac{1}{\sigma}\frac{d\sigma}{d\cos\theta'_{ab}} = \frac{1}{2}\left(1 + \alpha_a\alpha_b D_3\cos\theta'_{ab}\right)$$

being $\cos\theta'_{ab} \equiv \hat{p}_a \cdot \hat{p}'_b$

with inverted sign of n-component in one of the decay products

Conditions for entanglement

$$D = -\frac{(C_{kk} + C_{rr} + C_{nn})}{3} < -1/3$$

$$D_n = -\frac{(C_{kk} + C_{rr} - C_{nn})}{3} > +1/3$$

NLO predictions (parton-level)

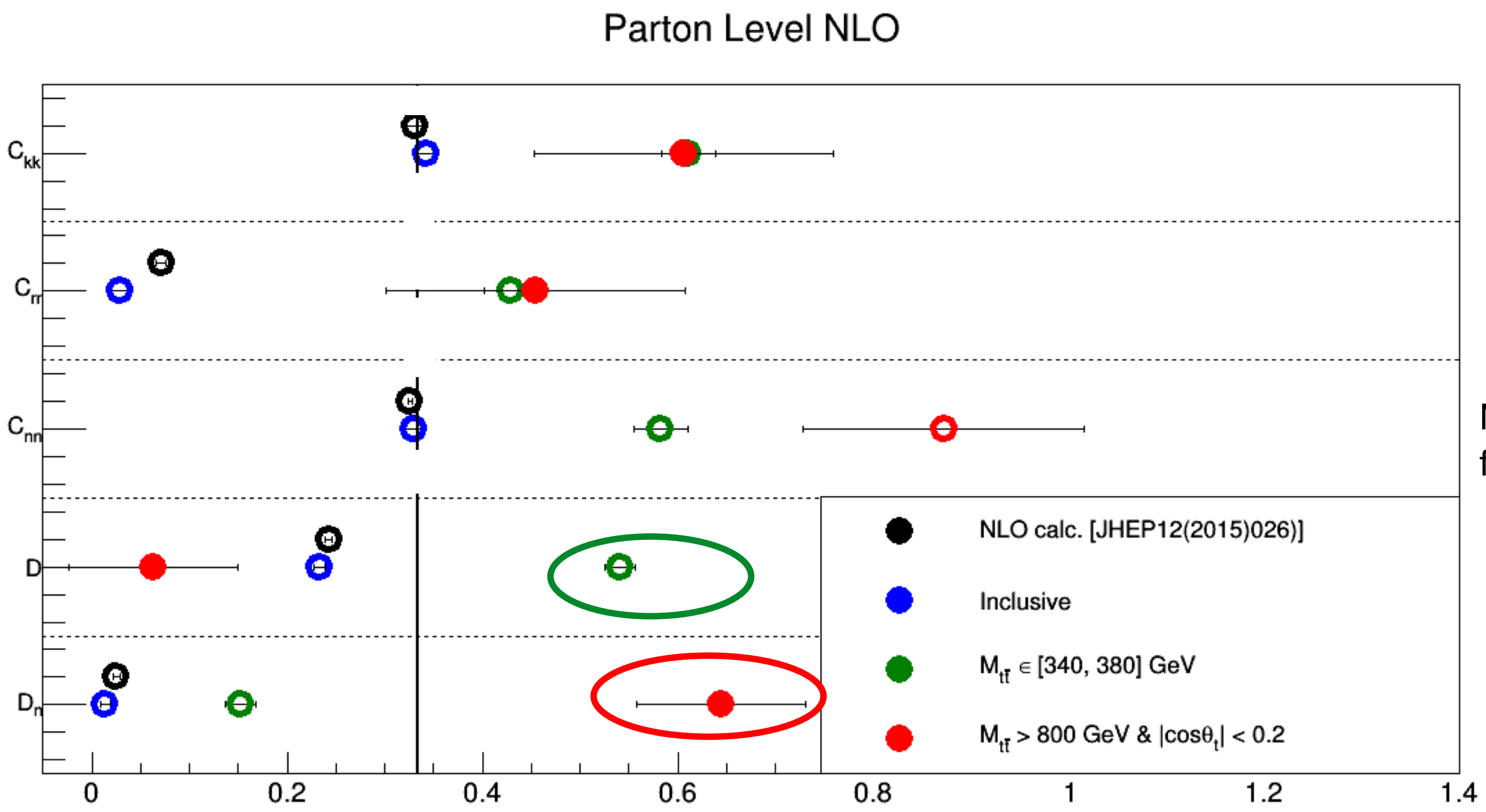

Empty circles: negative values

Note: Signs changed for Ci in the plot

Observable	Inclusive	Threshold	Boosted
Ckk	+0.342 ±0.009	+0.61 ±0.03	-0.60 ±0.15
Crr	+0.029 ±0.009	+0.42 ±0.03	-0.45 ± 0.15
Cnn	+0.329 ±0.009	+0.58 ±0.03	+0.87 ±0.14
D	-0.233 ±0.005	-0.54 ±0.02	+0.06 ±0.09
Dn	-0.014 ±0.005	-0.15 ±0.02	+0.64 ±0.09

Uncertainties quoted are due to limited MC statistics.

Theoretical unc. on these predictions not included (expected to be small).

ATLAS & CMS results

[1] Nature 633 (2024) 542
[2] arXiv:2406.03976
[3] arXiv:2409.11067

Channel	Threshold regime	Boosted regime
Dilepton	ATLAS (140/fb) >5σ [1] m_{tt}<380 GeV Particle-level CMS (36/fb) >5σ [2] m_{tt}<400 GeV & β_z<0.9 Parton-level	
Lepton+jets	CMS (140/fb) 2.2σ [3] m_{tt}<400 GeV Parton-level	CMS (140/fb) >5σ [3] m_{tt}>800 GeV & |cos(θ)|<0.4 Parton-level

CMS l+jets paper includes the full matrix measurements in various regions of the phase-space.

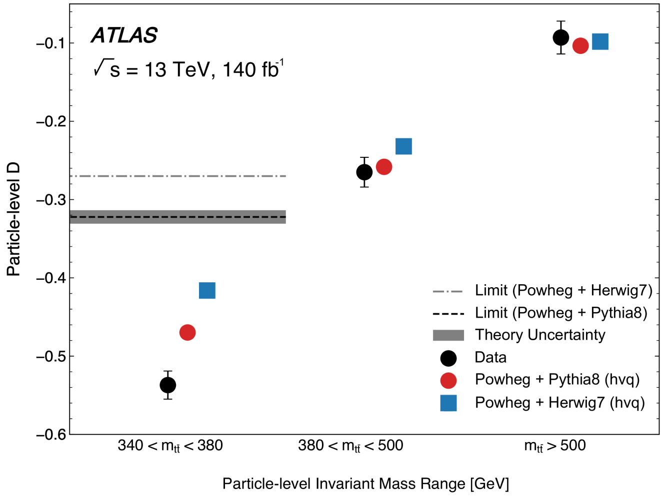

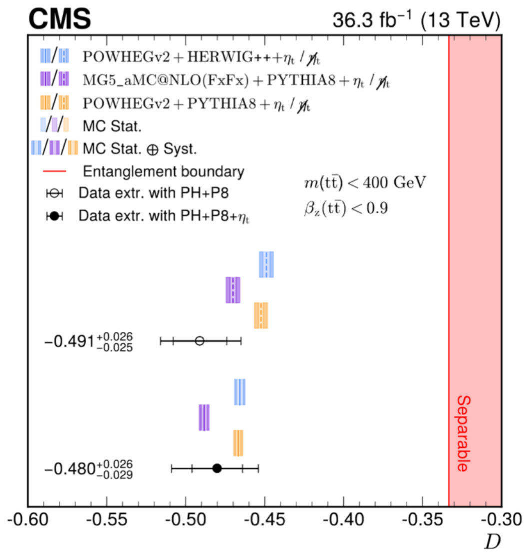

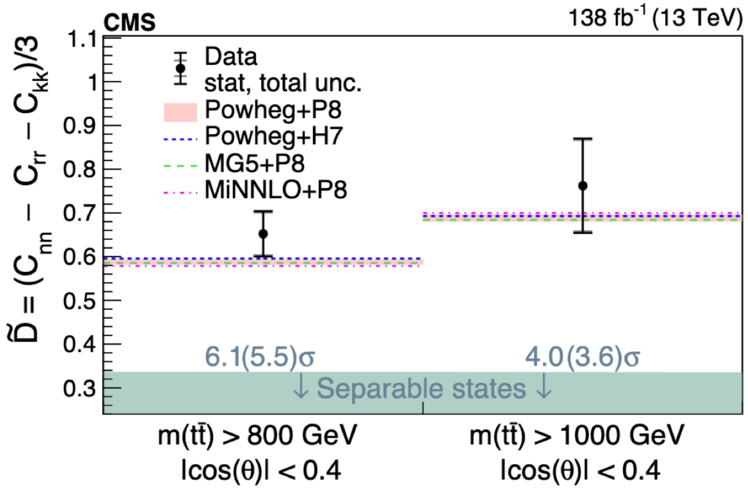

Understanding distorsions at detector-level

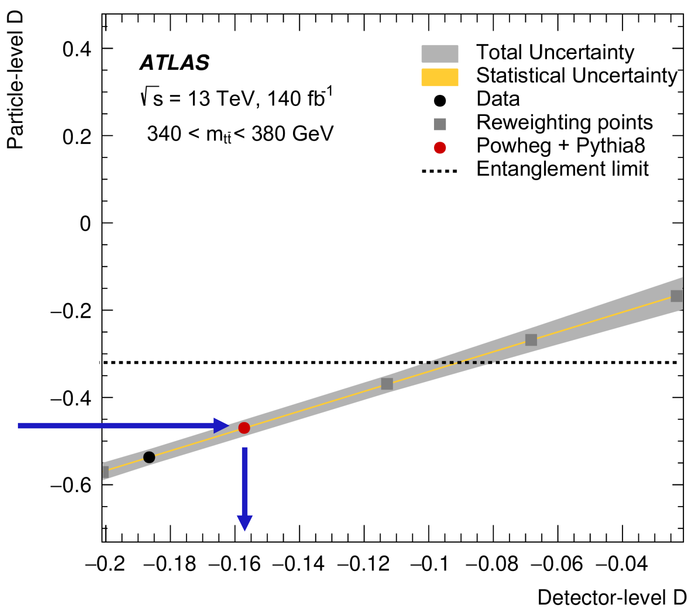

Nature 633 (2024) 542

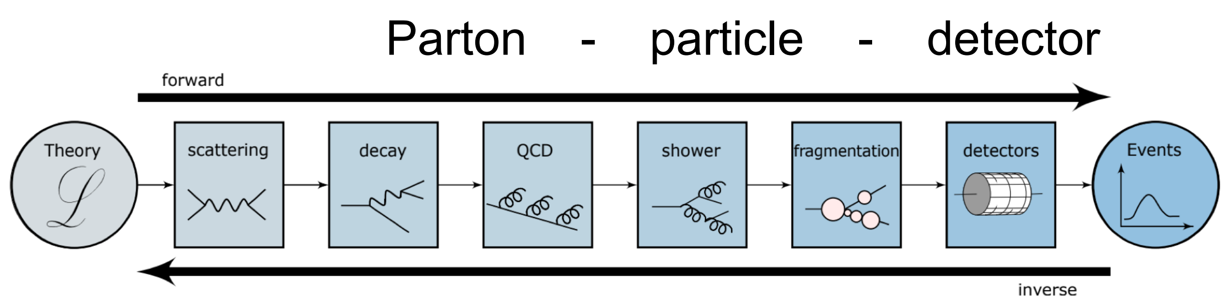

Sketch from SciPost Phys. 14, 079 (2023)

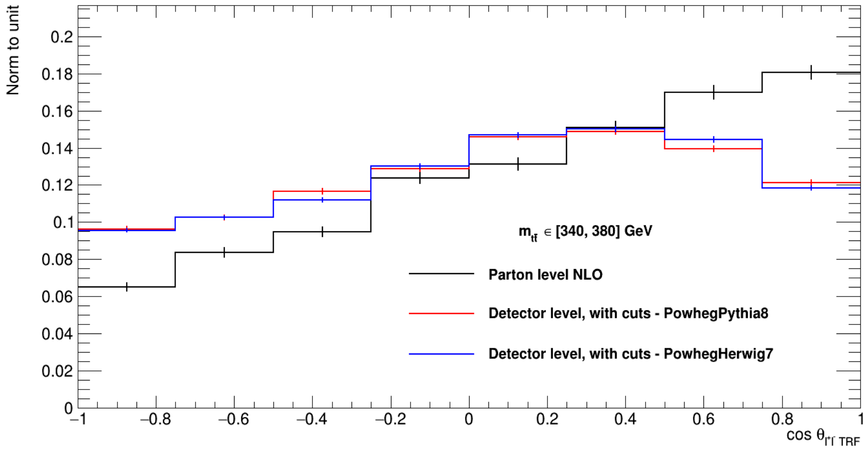

Parton level
Detector level - Powheg+Py8
Detector level - Powheg+Hw7

Note: Signs changed for Ci in the plot

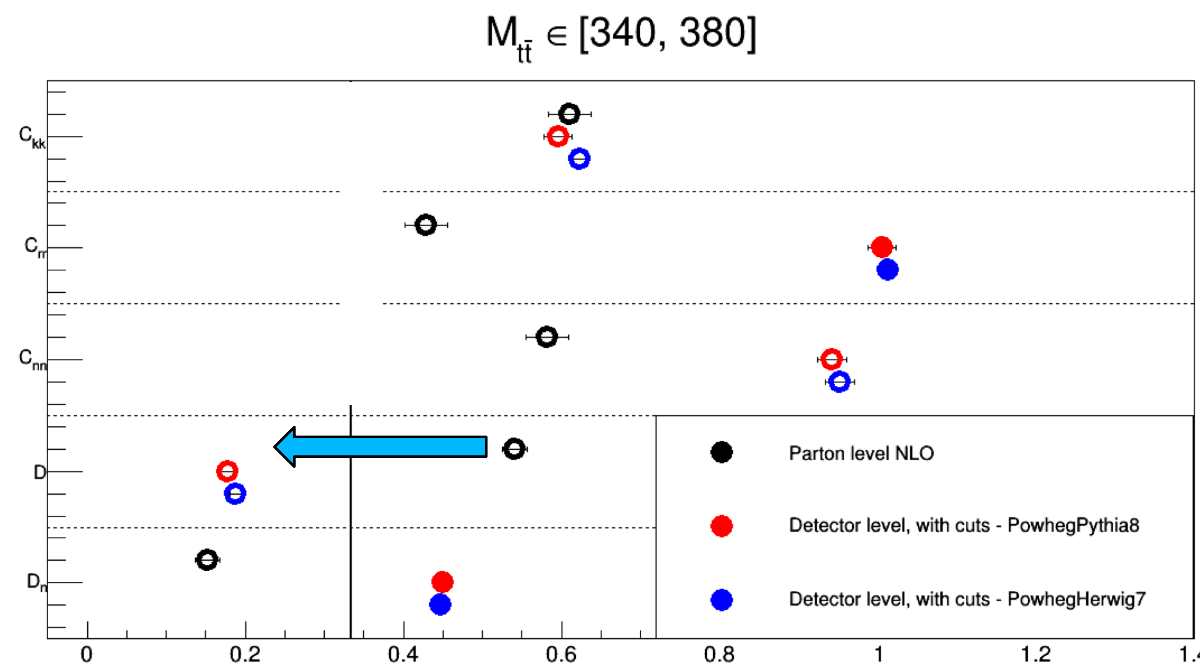

Migration effects: ~factor 3

using private ATLAS ntuples (thanks to Luis Monsonis); cuts on leptons and b-jets as well as top-quark reconstruction different to those used in the ATLAS published results

	Parton-level	Detector-level	Migration factor
D – threshold regime	-0.54 ±0.02	-0.177 ±0.009	~3
Dn – boosted regime	0.64 ±0.09	0.42 ±0.03	~1.5

Effect reduced in boosted regime

Parton vs detector level (dilepton channel, no cuts on m_{tt})

CUT SELECTION	$p_T(jet)$(GeV)	p_T(l)(GeV)	$\eta_{jet,l}$
BASE	>25	>27	$-2.5 < \eta_{jet,l} < 2.5$
p_T(l)	>25	>10	$-2.5 < \eta_{jet,l} < 2.5$
No η cut	>25	>27	-
CARDS SELECTION			
BASE	Default ATLAS Delphes Cards		
B-tag	light-jet mistagging rate c-jet mistagging rate b-tagging efficiency	Decreased ~50% Decreased ~75% Increased ~10%	
Jet reso	Jet resolution	Increased ~50%	
NEUTRINO SELECTION			
BASE	MET + neutrino weighting method		
Real ν + WM	Real ν summed + neutrino weighting method		
Real ν	Real ν		

Understanding causes of reconstruction level smearing

Study carried out with Delphes

Observable	PARTON LEVEL		RECONSTRUCTION LEVEL						
	No cuts	Base	Base	$p_t(l)$	No η cut	B-tag	Jet reso	Real ν + WM	Real ν
C_{kk}	-0.342	-0.43	-0.087	-0.001	-0.087	-0.088	-0.087	-0.082	-0.285
C_{rr}	-0.029	-0.04	-0.130	-0.119	-0.131	-0.131	-0.130	-0.110	-0.027
C_{nn}	-0.329	-0.39	-0.331	-0.335	-0.331	-0.328	-0.314	-0.313	-0.399
D	-0.233	-0.287	-0.183	-0.151	-0.183	-0.182	-0.177	-0.168	-0.237
D_3	-0.014	-0.029	0.038	0.072	0.038	0.036	0.034	0.040	0.029

The method used to reconstruct each individual neutrino is key to mitigate migration effects.

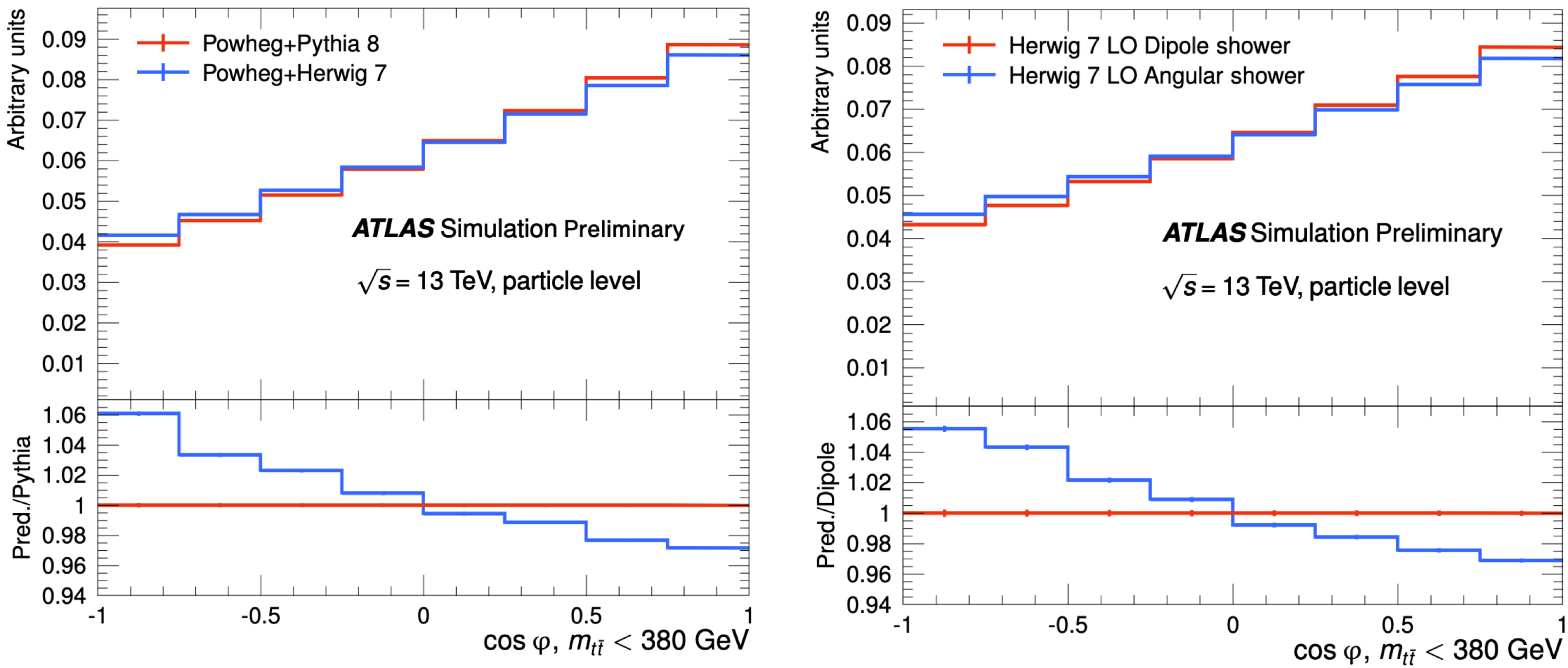

Notable differences seen at particle-level for two different parton-shower models

Nature 633 (2024) 542

Setting bounds in top SMEFT operators (using CMS results at parton-level)

follow-up from results in JHEP02(2022)032 & arXiv: 2205.02140

14 four-fermion op.

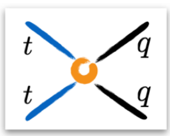

LL, RR

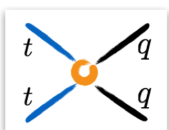

LR, RL

8 two-fermion op.

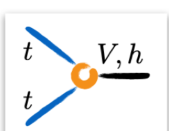

parameter	$t\bar{t}$	single t	tW	tZ	t decay	$t\bar{t}Z$	$t\bar{t}W$
$C^{1,8}_{Qq}$	Λ^{-2}	–	–	–	–	Λ^{-2}	Λ^{-2}
$C^{3,8}_{Qq}$	Λ^{-2}	Λ^{-4} [Λ^{-2}]	–	Λ^{-4} [Λ^{-2}]	Λ^{-4} [Λ^{-2}]	Λ^{-2}	Λ^{-2}
C^8_{tu}, C^8_{td}	Λ^{-2}	–	–	–	–	Λ^{-2}	–
$C^{1,1}_{Qq}$	Λ^{-4} [Λ^{-2}]	–	–	–	–	Λ^{-4} [Λ^{-2}]	Λ^{-4} [Λ^{-2}]
$C^{3,1}_{Qq}$	Λ^{-4} [Λ^{-2}]	Λ^{-2}	–	Λ^{-2}	Λ^{-2}	Λ^{-4} [Λ^{-2}]	Λ^{-4} [Λ^{-2}]
C^1_{tu}, C^1_{td}	Λ^{-4} [Λ^{-2}]	–	–	–	–	Λ^{-4} [Λ^{-2}]	–
C^8_{Qu}, C^8_{Qd}	Λ^{-2}	–	–	–	–	Λ^{-2}	–
C^8_{tq}	Λ^{-2}	–	–	–	–	Λ^{-2}	Λ^{-2}
C^1_{Qu}, C^1_{Qd}	Λ^{-4} [Λ^{-2}]	–	–	–	–	Λ^{-4} [Λ^{-2}]	–
C^1_{tq}	Λ^{-4} [Λ^{-2}]	–	–	–	–	Λ^{-4} [Λ^{-2}]	Λ^{-4} [Λ^{-2}]
$C^-_{\phi Q}$	–	–	–	Λ^{-2}	–	Λ^{-2}	–
$C^3_{\phi Q}$	–	Λ^{-2}	Λ^{-2}	Λ^{-2}	Λ^{-2}	–	–
$C_{\phi t}$	–	–	–	Λ^{-2}	–	Λ^{-2}	–
$C_{\phi tb}$	–	Λ^{-4}	Λ^{-4}	Λ^{-4}	Λ^{-4}	–	–
C_{tZ}	–	–	–	Λ^{-2}	–	Λ^{-2}	–
C_{tW}	–	Λ^{-2}	Λ^{-2}	Λ^{-2}	Λ^{-2}	–	–
C_{bW}	–	Λ^{-4}	Λ^{-4}	Λ^{-4}	Λ^{-4}	–	–
C_{tG}	Λ^{-2}	[Λ^{-2}]	Λ^{-2}	–	[Λ^{-2}]	Λ^{-2}	Λ^{-2}

JHEP02(2020)131

ATLAS & CMS results

[1] Nature 633 (2024) 542
[2] arXiv:2406.03976
[3] arXiv:2409.11067

Channel	Threshold regime	Boosted regime
Dilepton	ATLAS (140/fb) >5σ [1] m_{tt}<380 GeV Particle-level **CMS (36/fb) >5σ [2]** **m_{tt}<400 GeV & β_z<0.9** **Parton-level**	
Lepton+jets	CMS (140/fb) 2.2σ [3] m_{tt}<400 GeV Parton-level	**CMS (140/fb) >5σ [3]** **m_{tt}>800 GeV & |cos(θ)|<0.4** **Parton-level**

CMS l+jets paper includes the full matrix measurements in various regions of the phase-space.

Here we have just explored the threshold and boosted regimes. More to explore in terms of EFT…

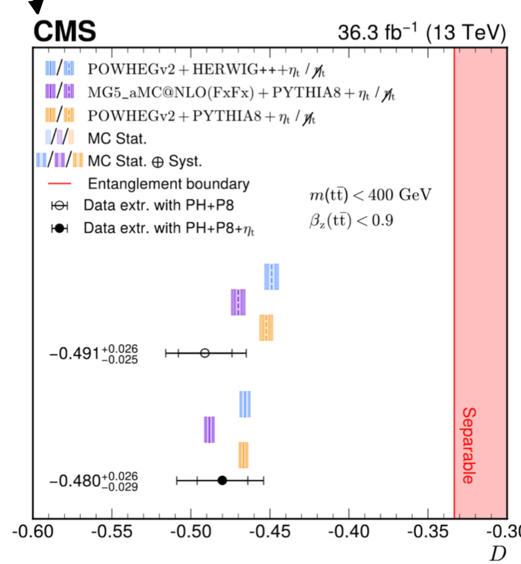

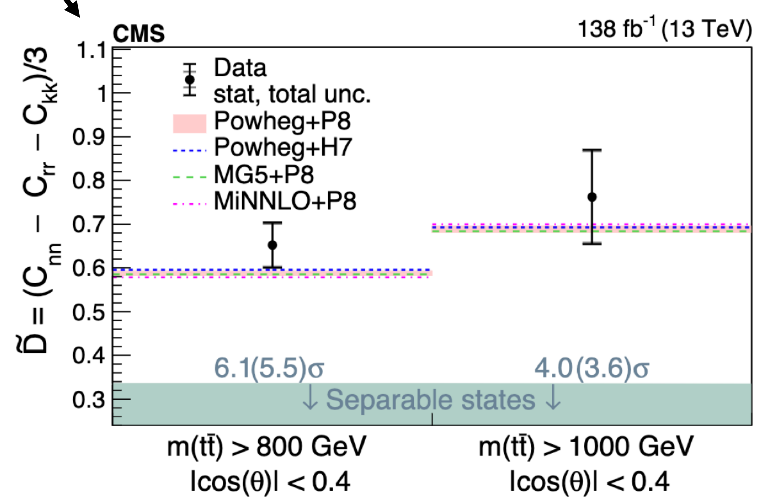

$$X = X_{SM} + \boxed{\frac{1}{\Lambda^2}\sum_i C_i X_i^{(1)}} + \boxed{\frac{1}{\Lambda^4}\sum_{ij} C_i C_j X_{ij}^{(2)}} + \mathcal{O}(\Lambda^{-4})$$

Linear Terms   Quadratic Terms

Dependence derived with
MadGraph5_aMC@NLO & SMEFT@NLO

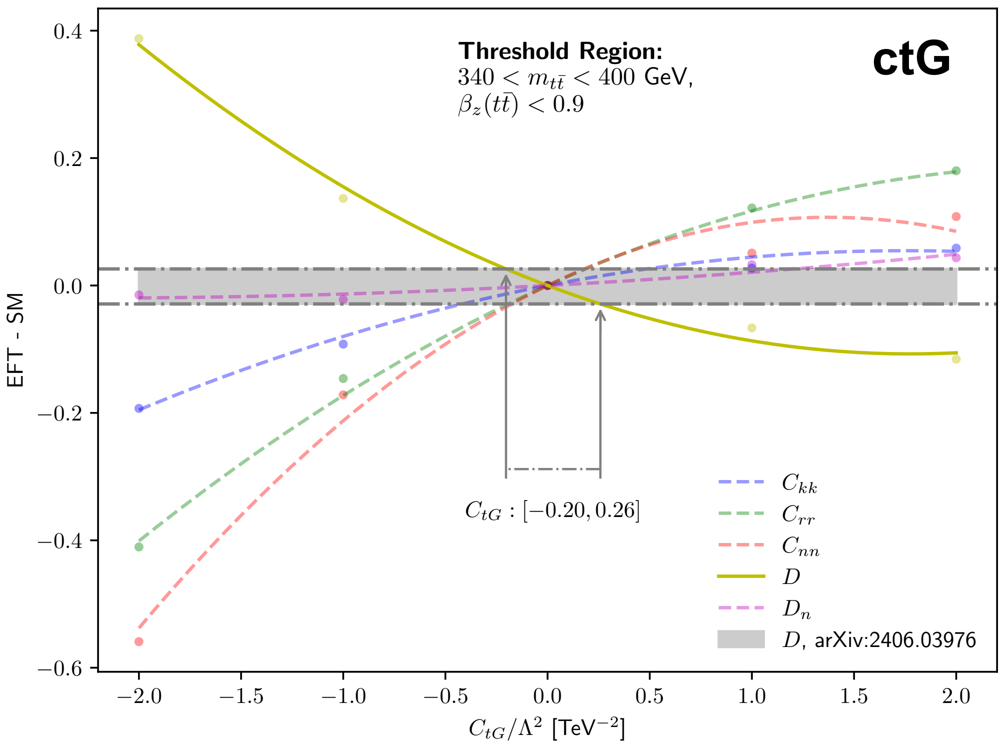

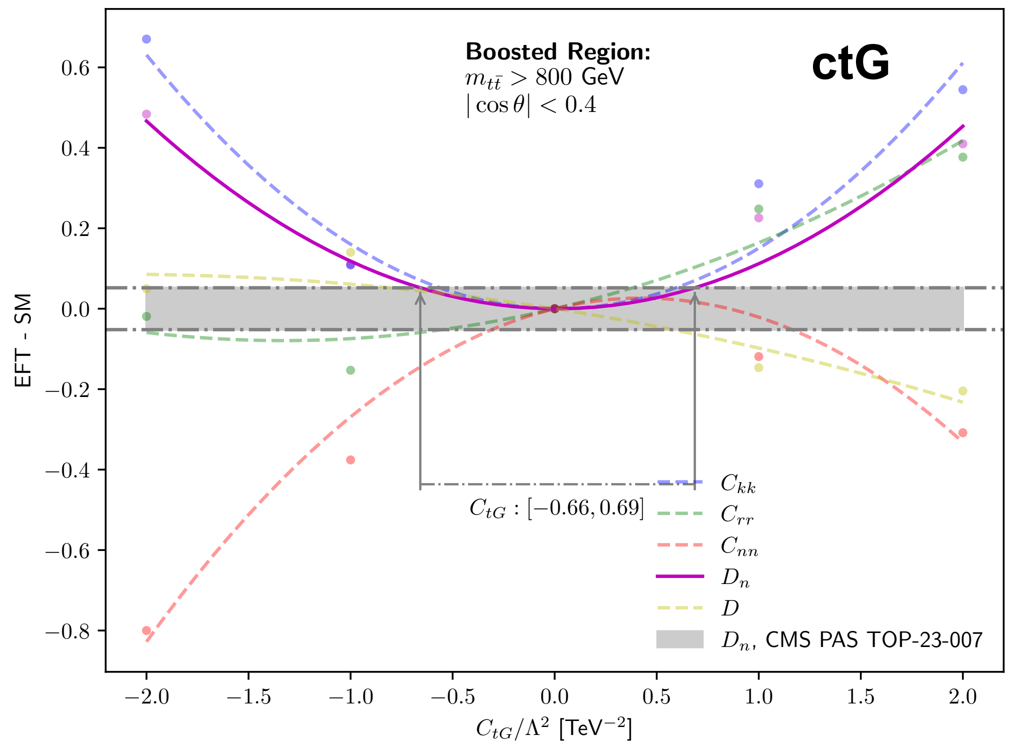

- From D → $c_{tG}/\Lambda^2 \in [-0.20, 0.26]$ TeV^{-2} @ 68%CL
- C_{nn} seems also sensitive in threshold regime

- From D_n → $c_{tG}/\Lambda^2 \in [-0.66, 0.69]$ TeV^{-2} @ 68%CL
- C_{kk} and C_{nn} also sensitive in boosted regime

Sensitivity on O_{tG} operator from various observables

Individual limits

Linear+Quad.

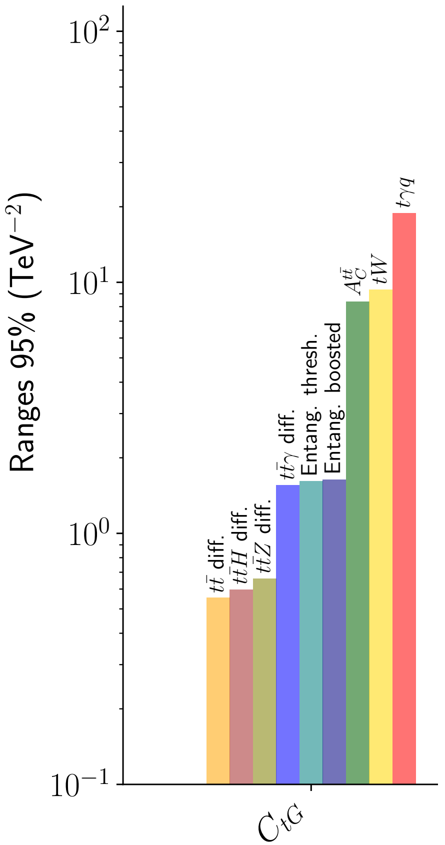

Only linear

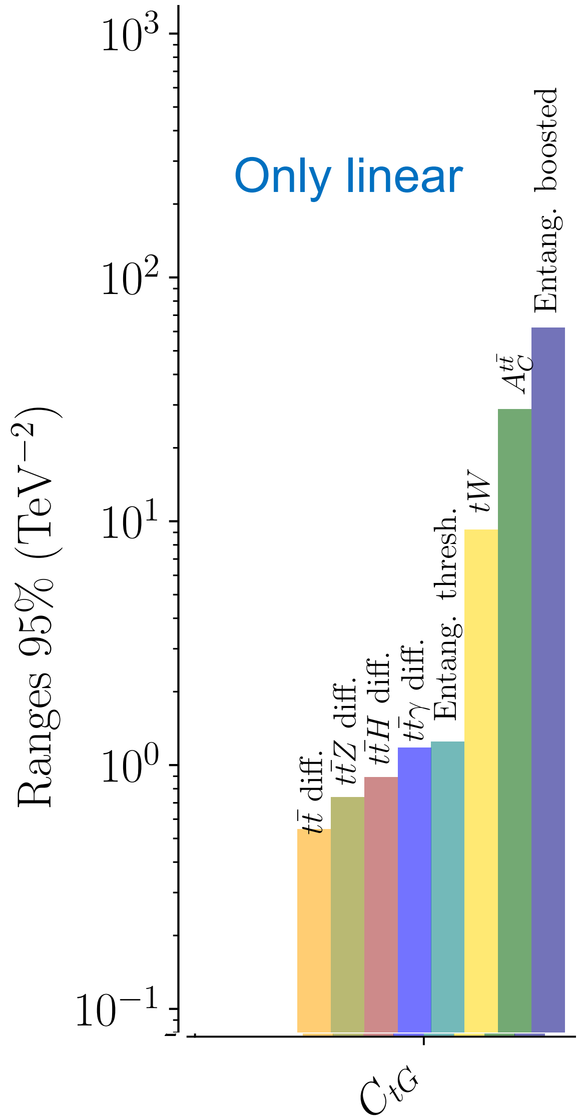

- Sensitivity from D @ threshold and D_n @ boosted compared to that from other observables: differential cross-sections in tt, diff. tt charge-asymmetry, diff. ttZ σ, diff. tty σ, ttH σ
- New entanglement observables may help to resolve blind directions
- When including only linear terms, bounds from D_n are degraded significantly

Sensitivity on O_{tG} operator from various observables

Individual limits

Linear+Quad.

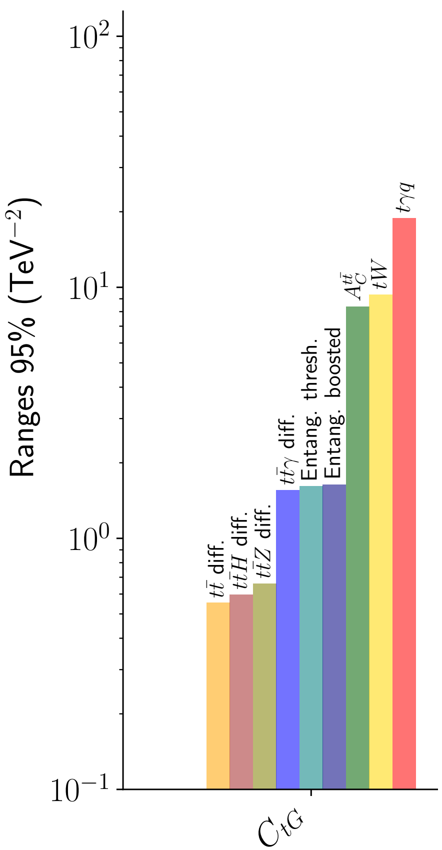

Only linear

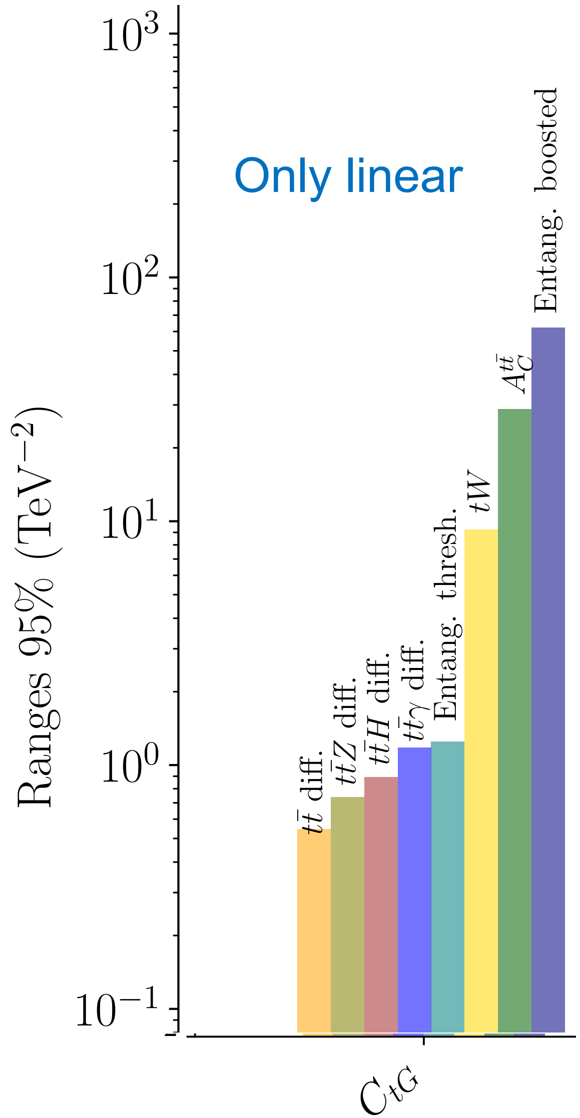

Global limits

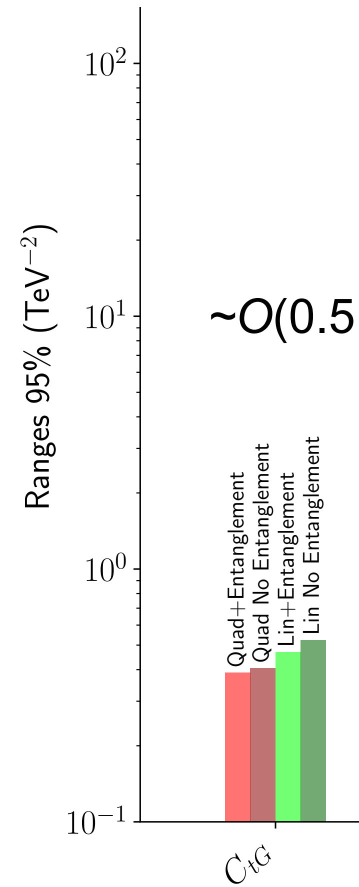

~O(0.5 TeV^{-2})

- Sensitivity from D @ threshold and D_n @ boosted compared to that from other observables: differential cross-sections in tt, diff. tt charge-asymmetry, diff. ttZ σ, diff. ttγ σ, ttH σ
- New entanglement observables may help to resolve blind directions
- When including only linear terms, bounds from D_n are degraded significantly

Sensitivity on 4F operators from various observables

Linear+Quad. limits

ctG and 4F- octets

O(1-10 TeV^{-2})

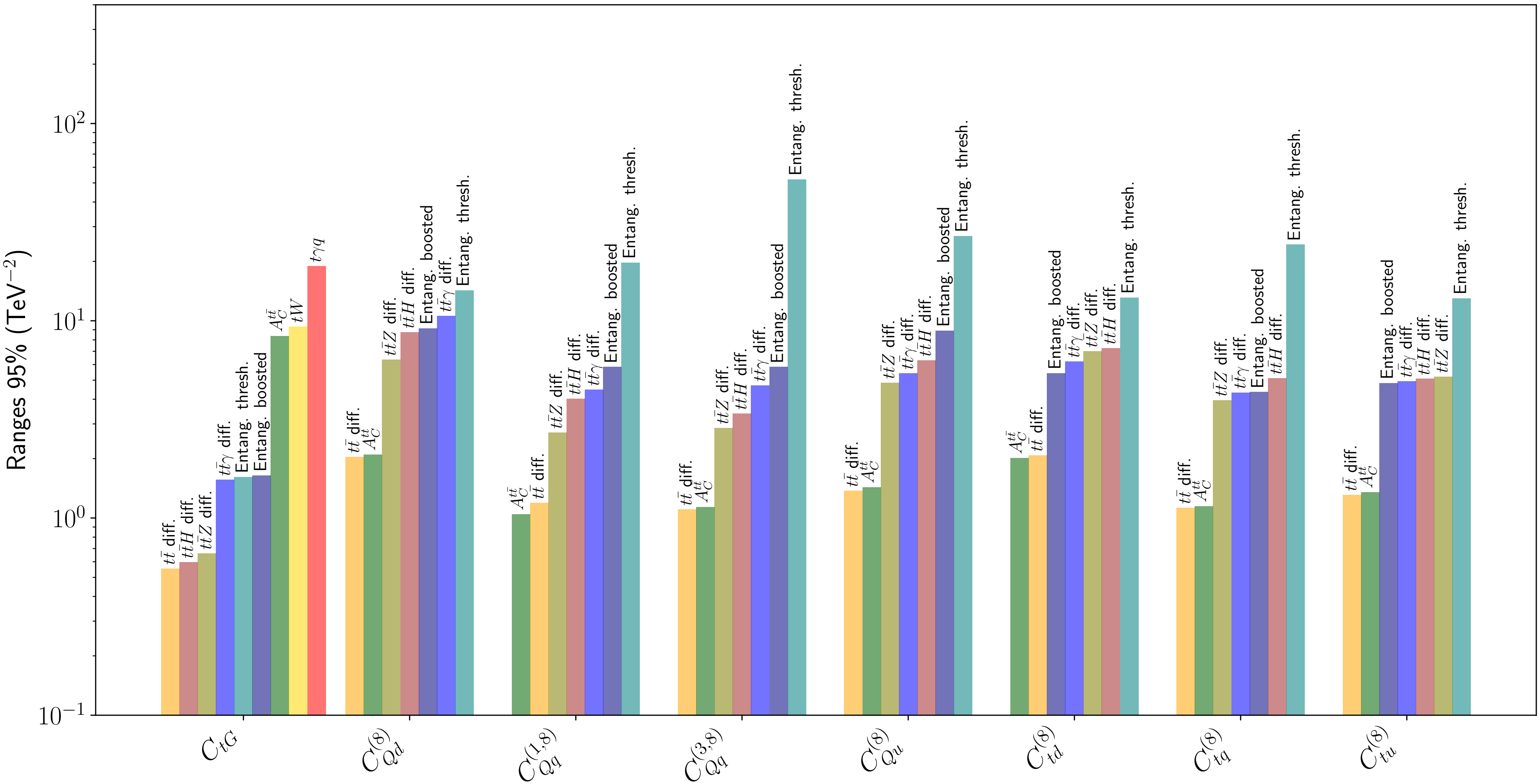

- Individual limits obtained from these two entanglement observables are still not very competitve, but may help to resolve blind directions

Sensitivity on 4F operators from various observables

Linear limits

ctG and 4F- octets

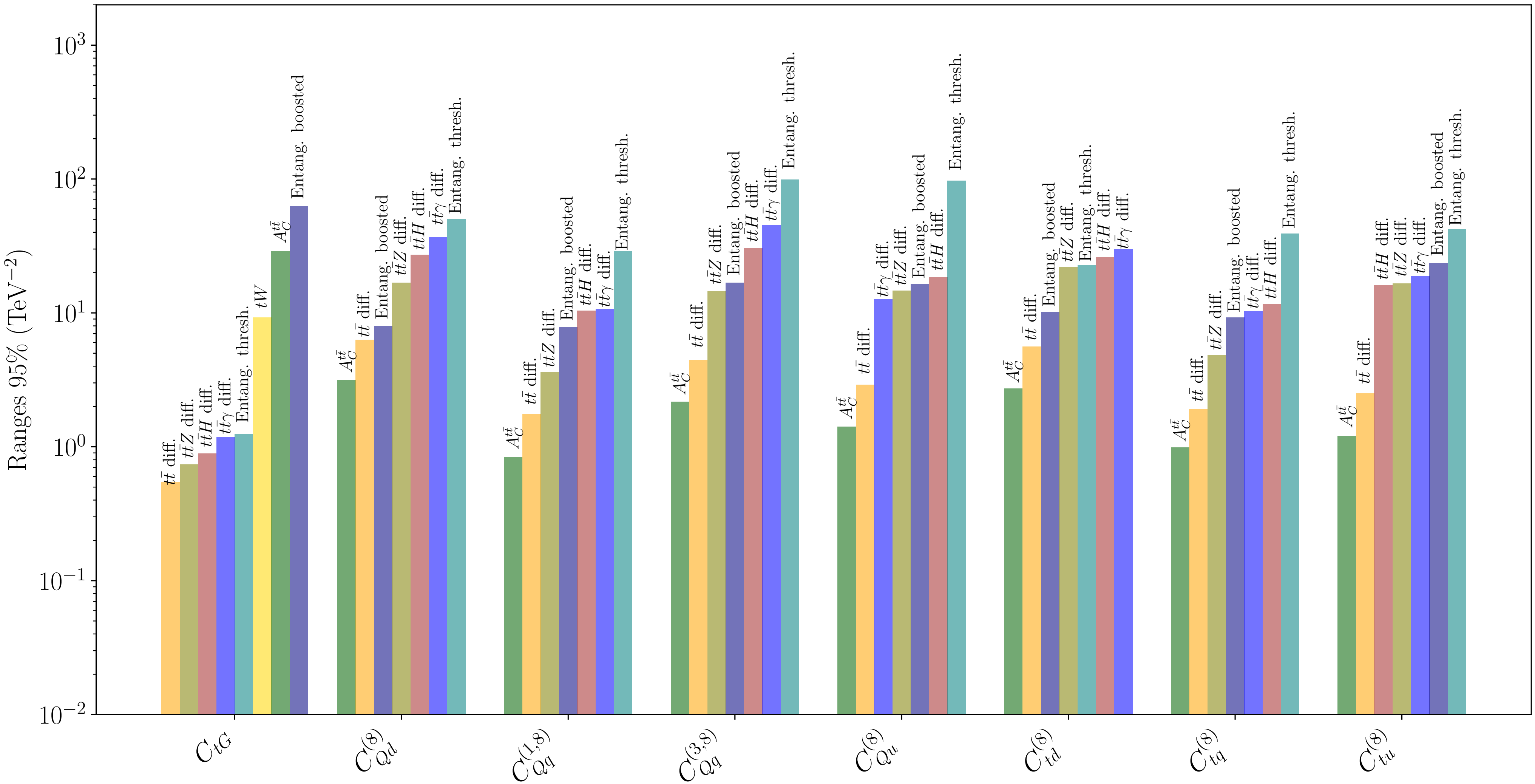

- Limits degraded when considering only linear terms

Sensitivity on global fits from those observables

ctG and 4F- octets

VERY PRELIMINARY

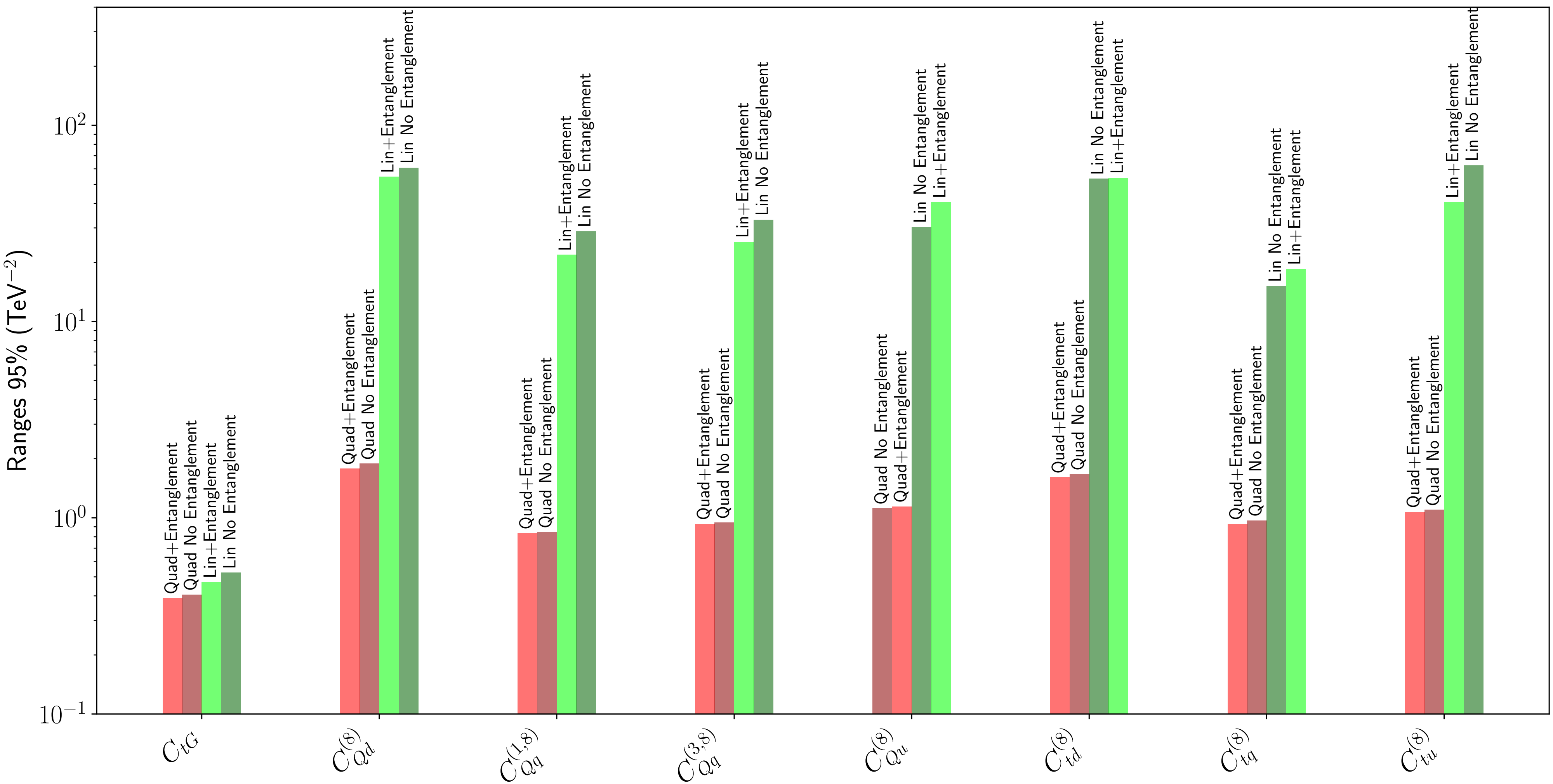

Summary

Understanding parton-to-detector level migration effects

- Migration effects ~factor 3 in threshold region; seem to be smaller in the boosted regime
- The method used to reconstruct each neutrino in dilepton events is key to mitigate migration effects
- Need to understand differences seen by ATLAS at particle-level for two different parton-shower models

SMEFT bounds

- SMEFT new interactions modify both conventional and quantum observables
    - Dimension-6 operators can modify the degree of entanglement between top quarks

- Recently measured observables can break degeneracies between operators when combined with other observables
    - Quadratic terms are very relevant

Next steps: global SMEFT analyses including these new available experimental results.

THANKS FOR YOUR ATTENTION

BACK-UP

Sensitivity on SMEFT operators from various observables

Linear+Quad. limits

4F-singlets

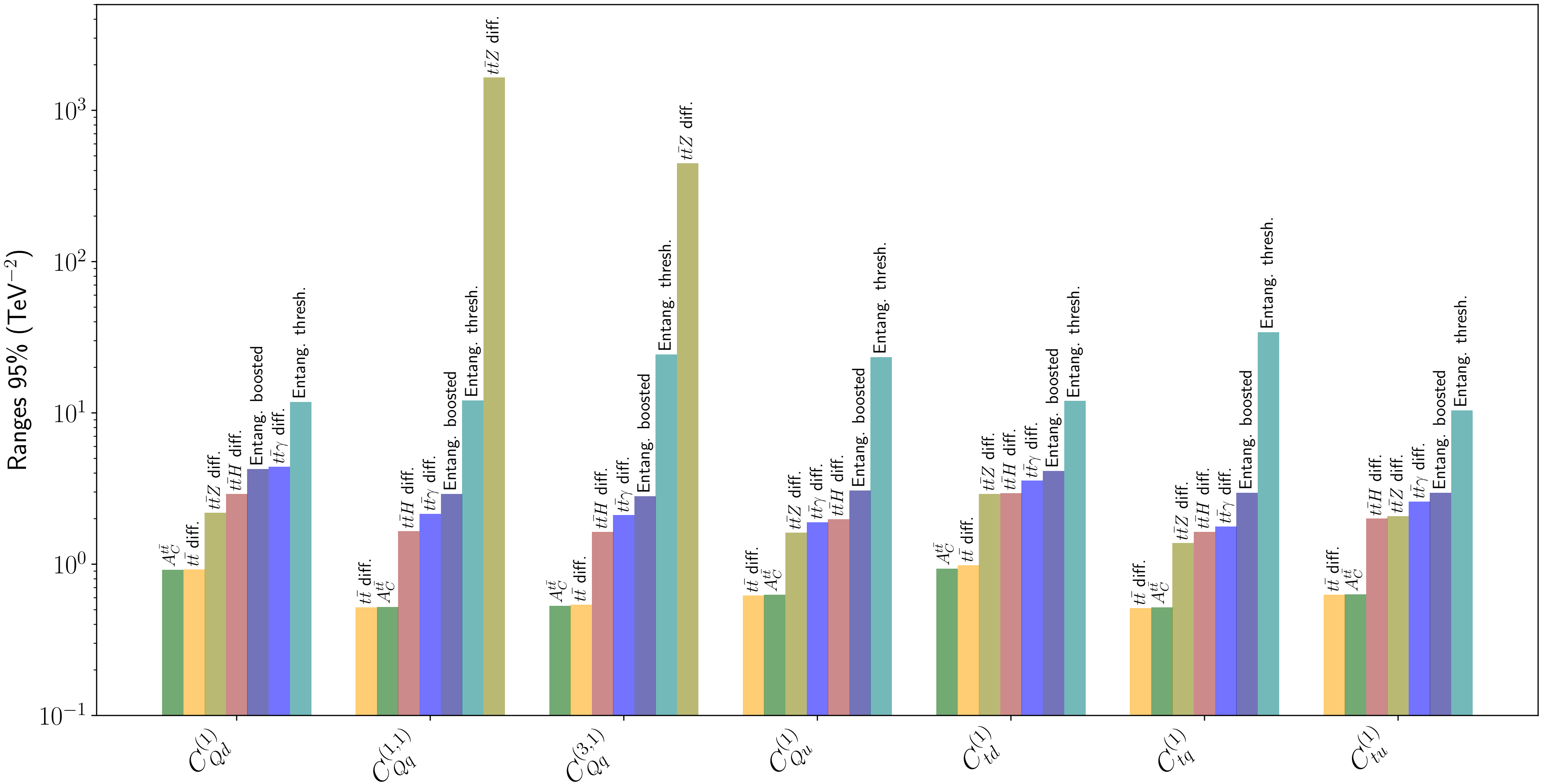

Sensitivity on SMEFT operators from various observables

Linear limits

4F-singlets

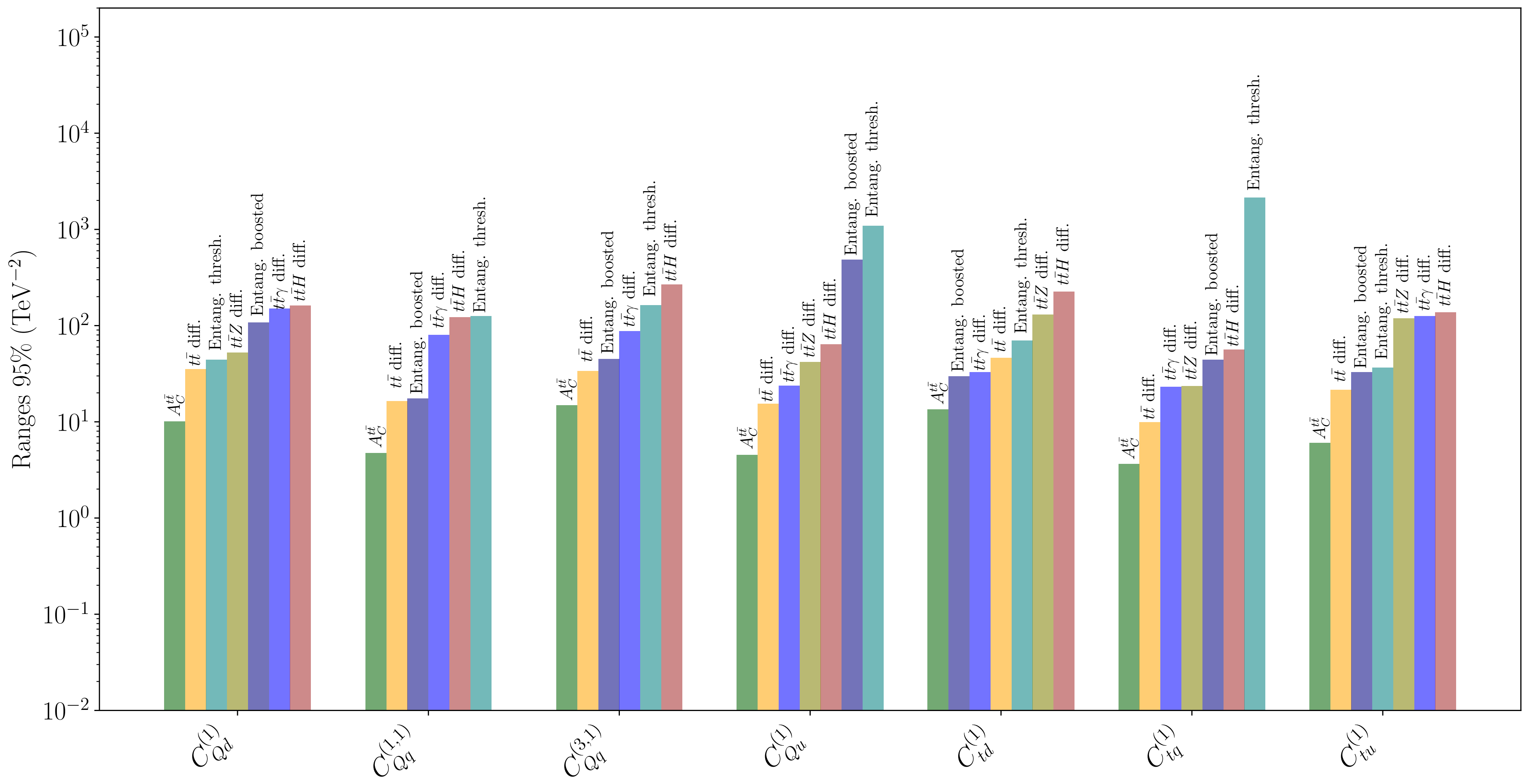

4F-singlets

VERY PRELIMINARY

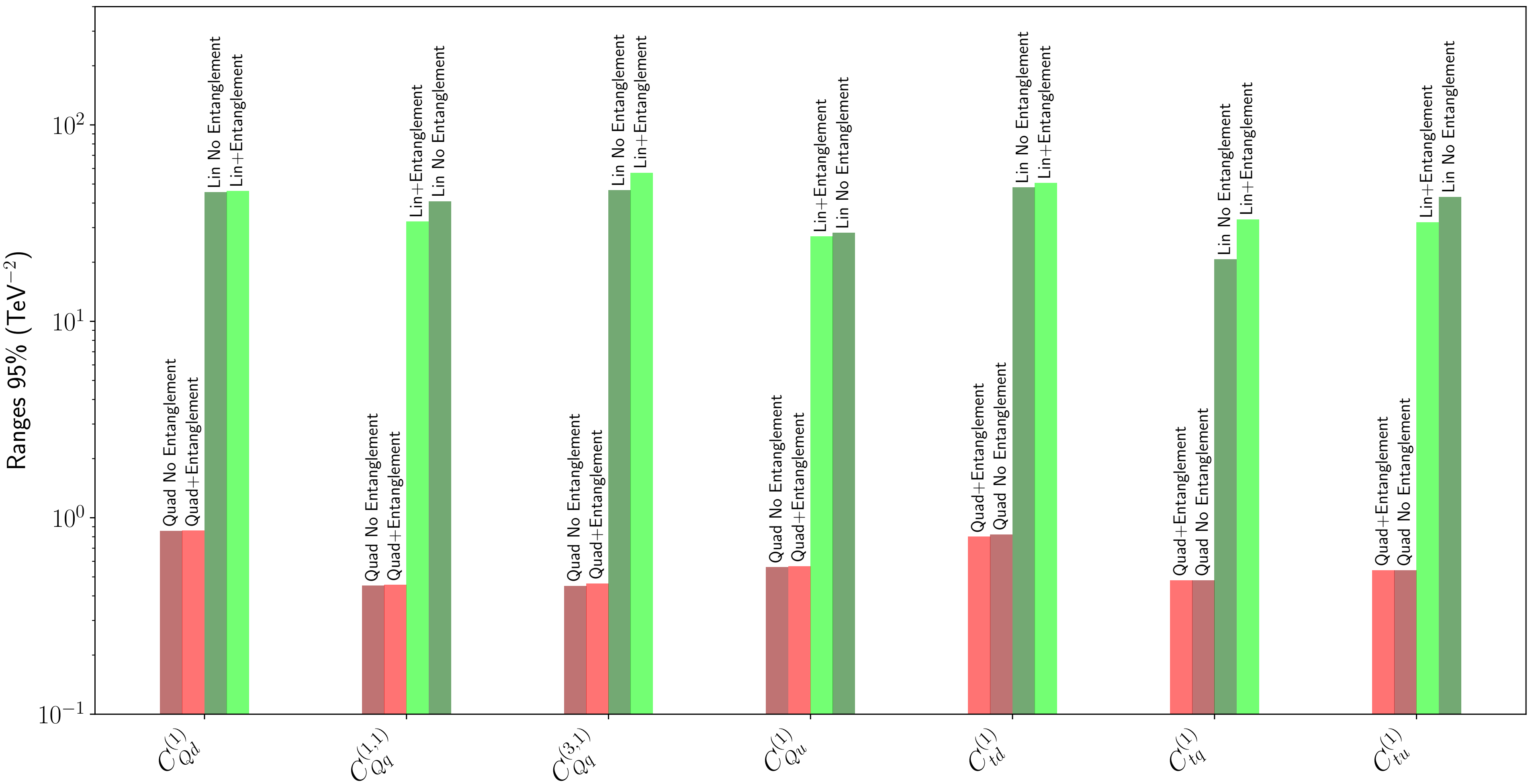

Sensitivity on global fits from those observables

ctG and 4F- octets

VERY PRELIMINARY

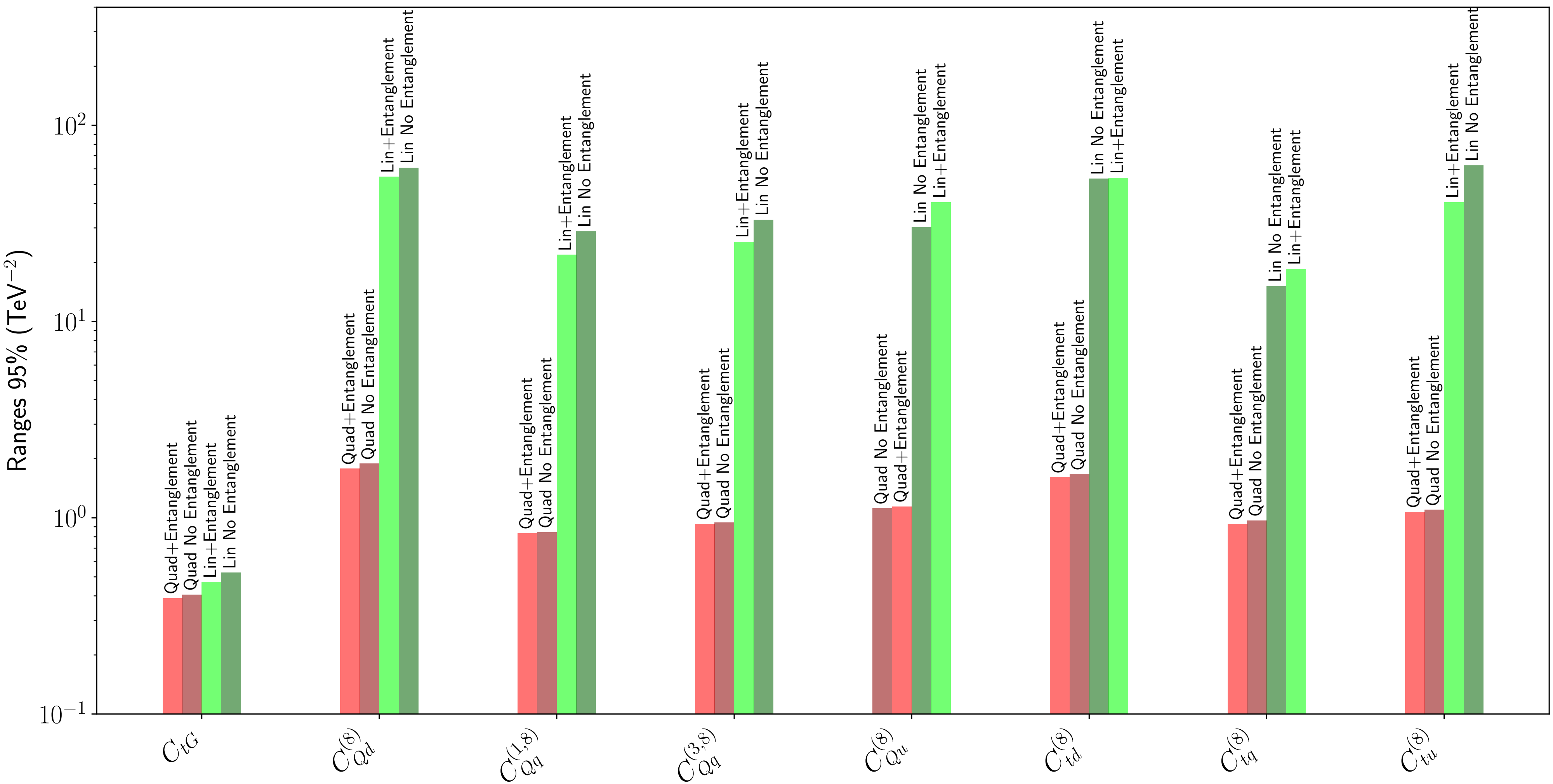

2σ individual limits (expected)

	from Dn (95%CL) linear	from D (95%CL) linear	from Dn (95%CL) linear+quad.	from D (95%CL) linear+quad.
ctG	[-32.14, 32.14]	[-0.43, 0.48]	[-0.94, 0.97]	[-0.39,0.57]
cQd(8)	[-4.20, 4.20]	[-19.76, 17.71]	[-2.72, 7.73]	[-8.15, 5.58]
cQq(1,8)	[-4.02, 4.02]	[-10.86, 9.73]	[-2.14, 4.59]	[-5.95, 13.16]
cQq(3,8)	[-8.71, 8.71]	[-33.90, 37.81]	[-2.71, 3.93]	[-17.16, 34.74]
cQu(8)	[-8.44, 8.44]	[-33.27, 37.11]	[-3.68, 6.52]	[-10.71, 15.80]
ctd(8)	[-5.19, 5.19]	[-8.66, 7.77]	[-2.25, 3.96]	[-8.80, 4.13]
ctq(8)	[-4.72, 4.72]	[-14.75, 13.22]	[-1.86, 3.08]	[-16.67, 7.37]
ctu(8)	[-12.08, 12.08]	[-16.09, 14.43]	[-2.45, 3.08]	[-5.03, 7.33]
cQd(1)	[-54.60, 54.60]	[-15.02, 16.75]	[-2.42, 2.53]	[-4.67, 6.77]
cQq(1,1)	[-8.97, 8.97]	[-47.74, 42.81]	[-1.85, 1.53]	[-6.17, 5.39]
cQq(3,1)	[-23.29, 23.29]	[-54.79, 61.11]	[-1.55, 1.66]	[-12.61, 10.45]
cQu(1)	[-255.15, 255.15]	[-371.69, 414.58]	[-1.76, 1.75]	[-11.10, 11.44]
ctd(1)	[-15.29, 15.29]	[-23.98, 26.74]	[-2.16, 2.51]	[-6.19, 5.03]
ctq(1)	[-22.72, 22.72]	[-777.28, 866.97] :)	[-1.78, 1.65]	[-16.40, 16.75]
ctu(1)	[-16.93, 16.93]	[-12.59, 14.04]	[-1.78, 1.61]	[-5.93, 4.17]

Sensitivity on SMEFT operators from those observables

4F octets @ boosted

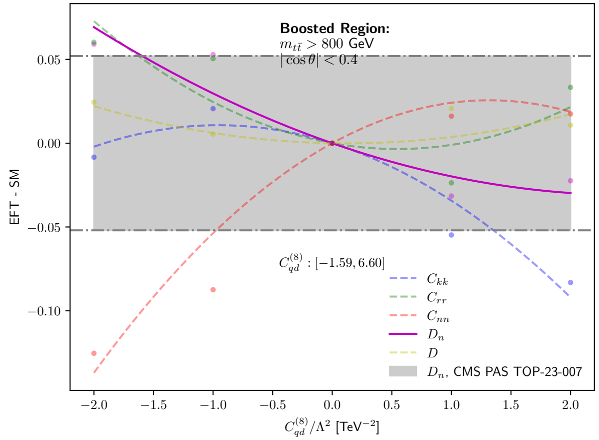

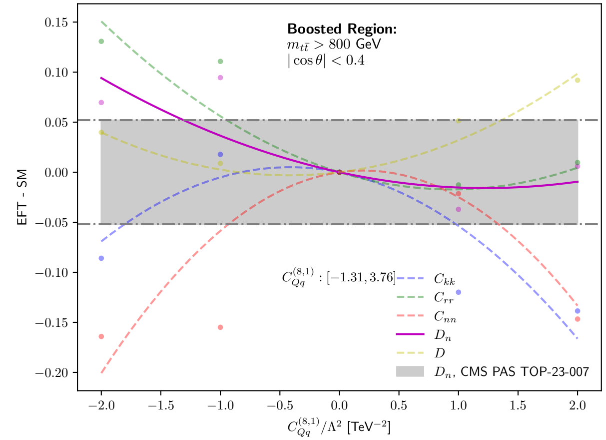

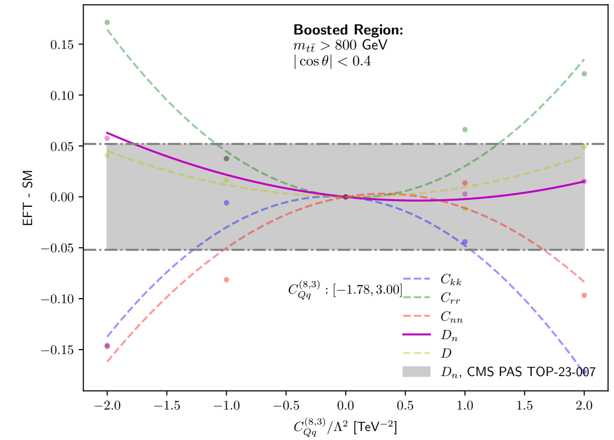

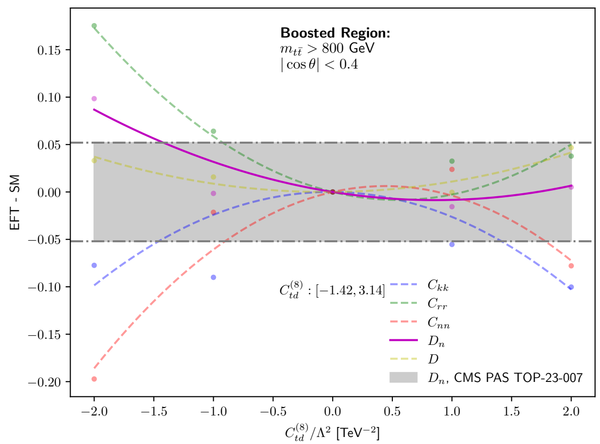

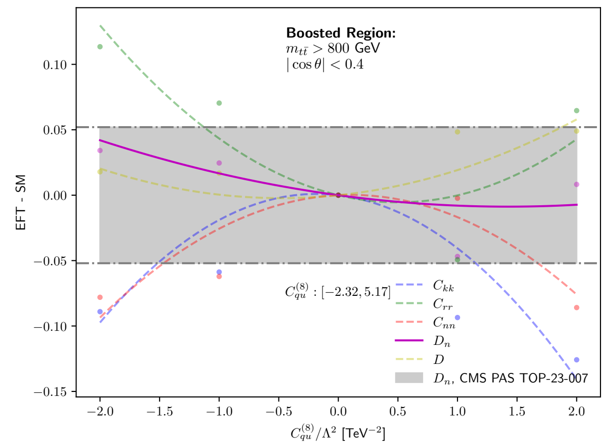

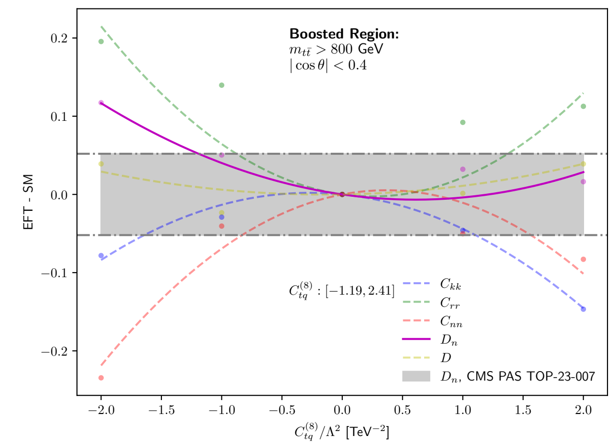

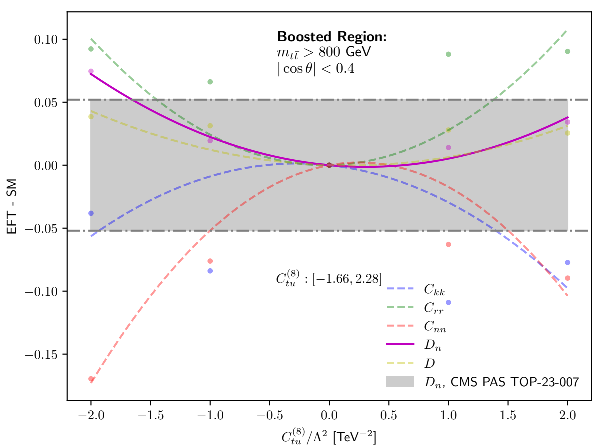

- Quadratic term quite relevant
- Crr, Ckk and Cnn seem quite sensitive in this regime

Sensitivity on SMEFT operators from those observables

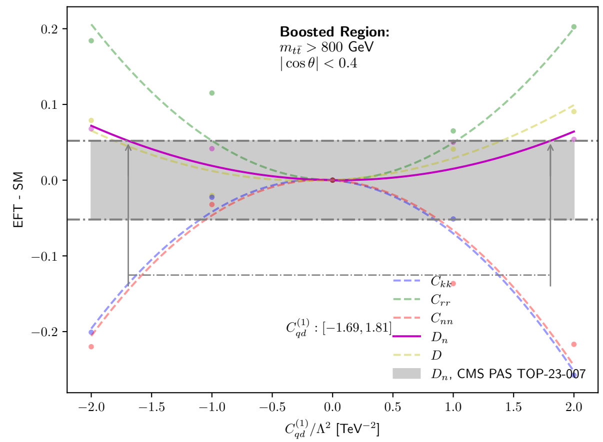

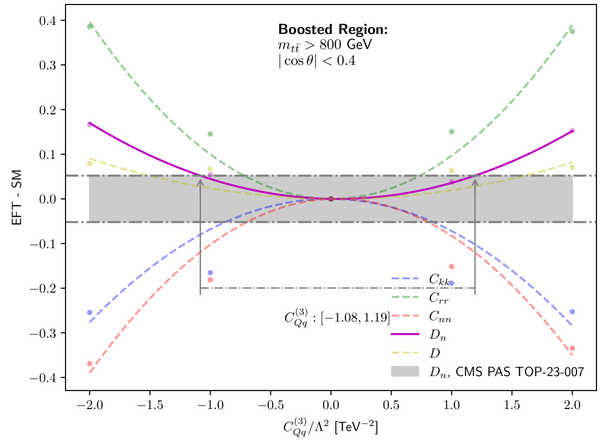

4F singlets @ boosted

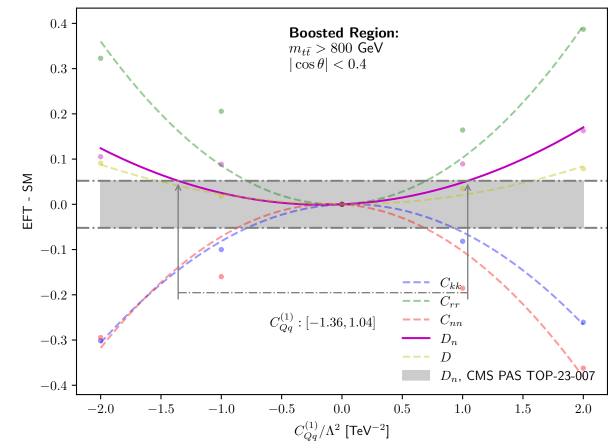

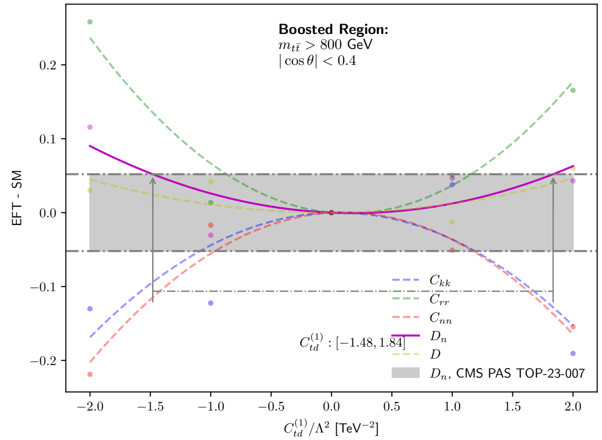

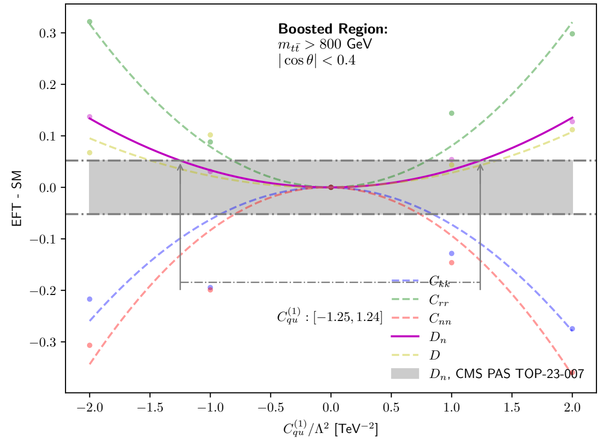

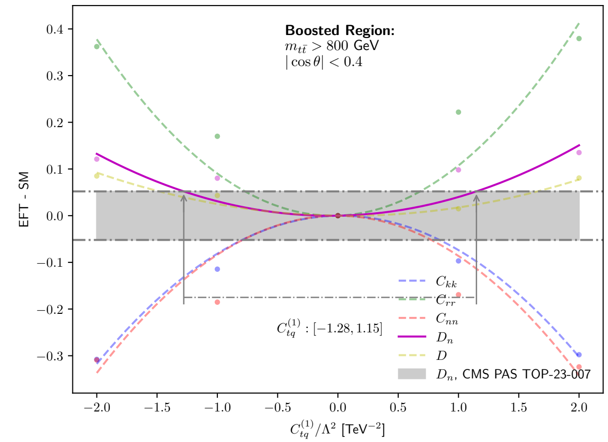

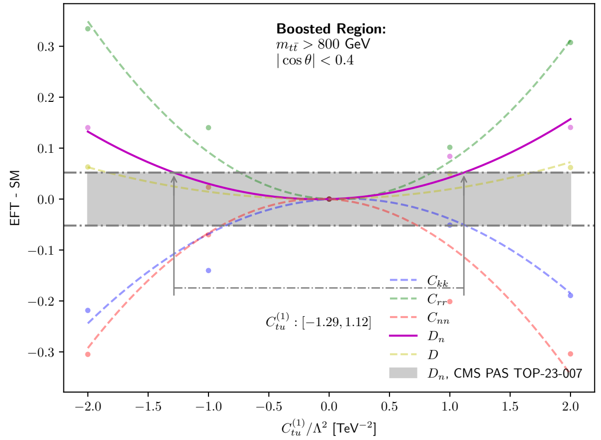

- Quadratic term quite relevant
- Crr, Ckk and Cnn seem quite sensitive in this regime

Sensitivity on SMEFT operators from those observables

Threshold - doublets

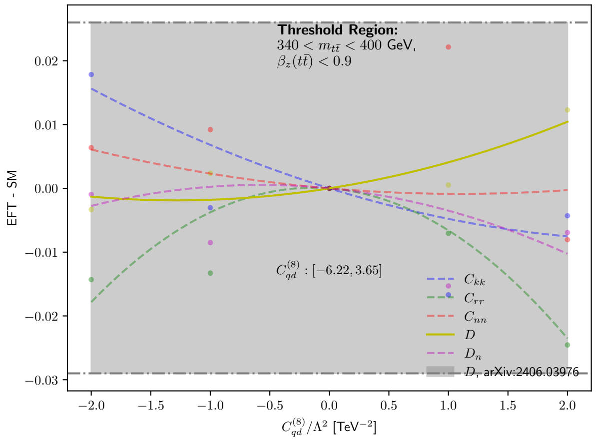

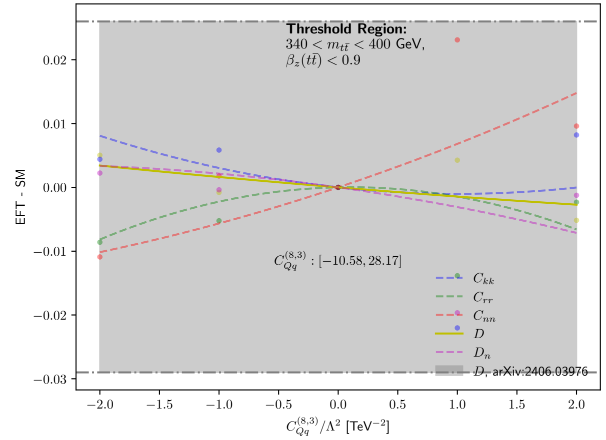

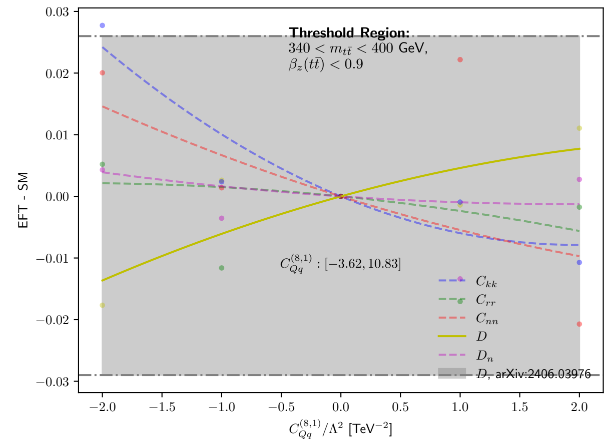

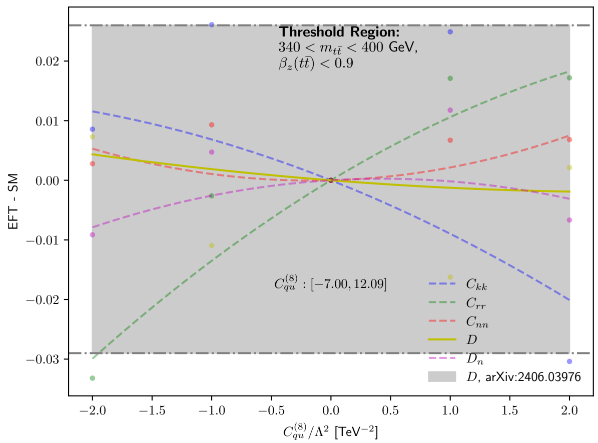

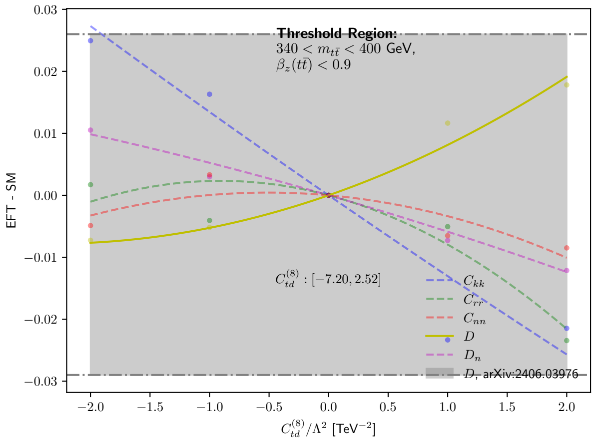

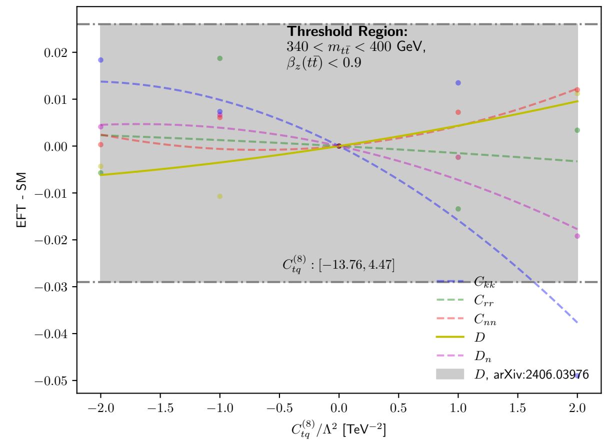

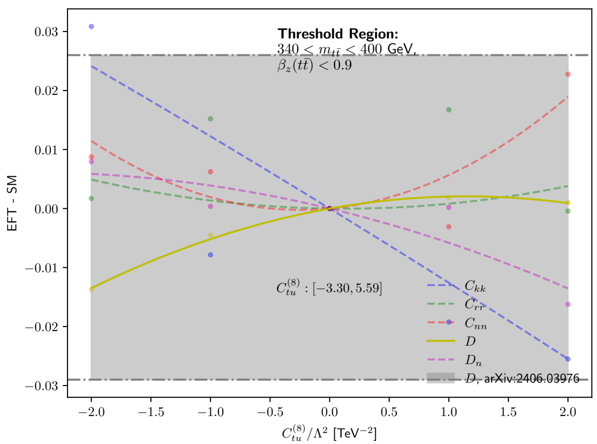

Quadratic term quite relevant

Sensitivity on SMEFT operators from those observables

Threshold - singlets

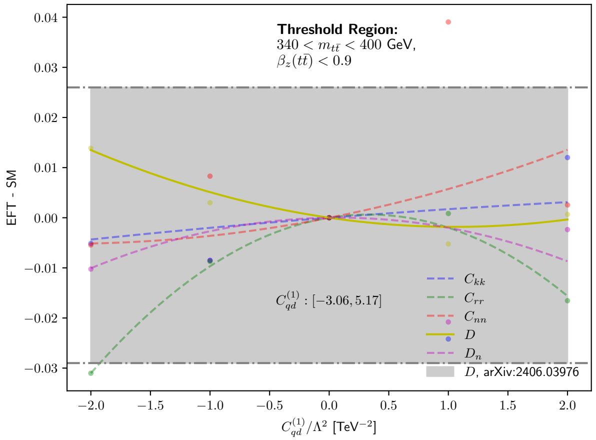

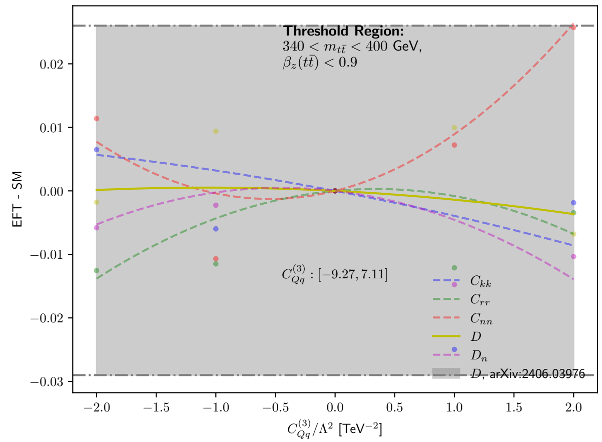

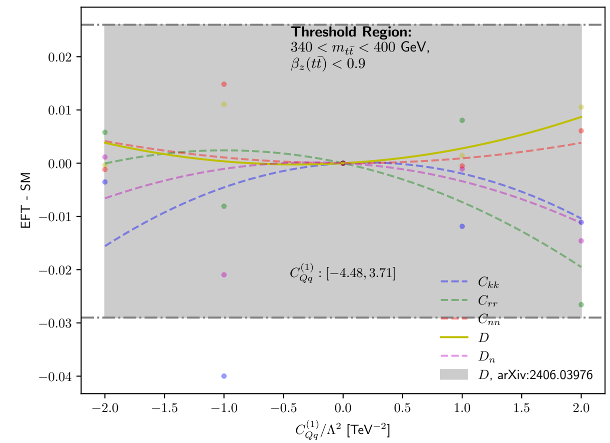

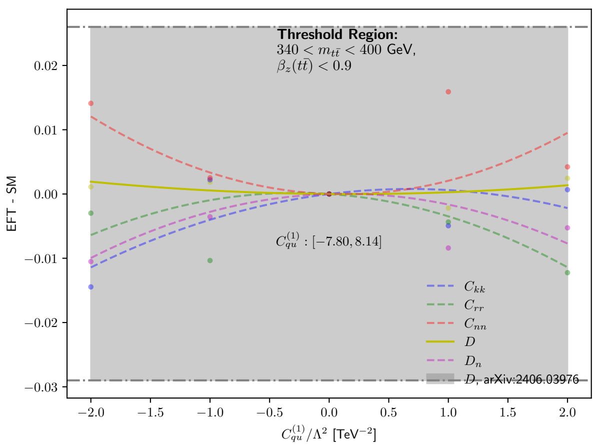

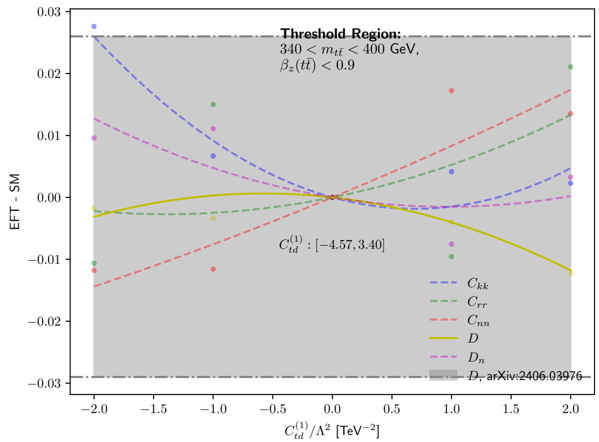

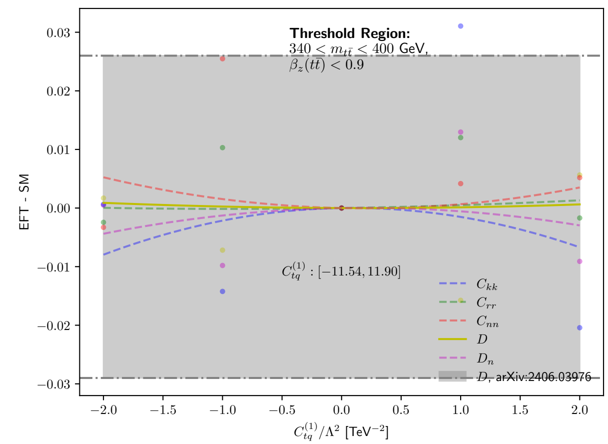

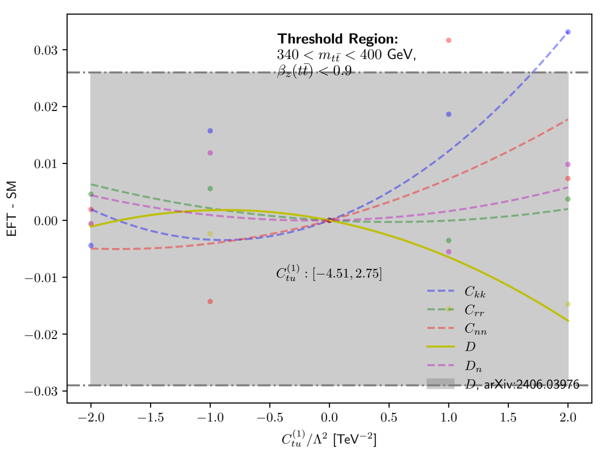

Quadratic term quite relevant

Distorsions at detector level (dilepton - boosted regime)

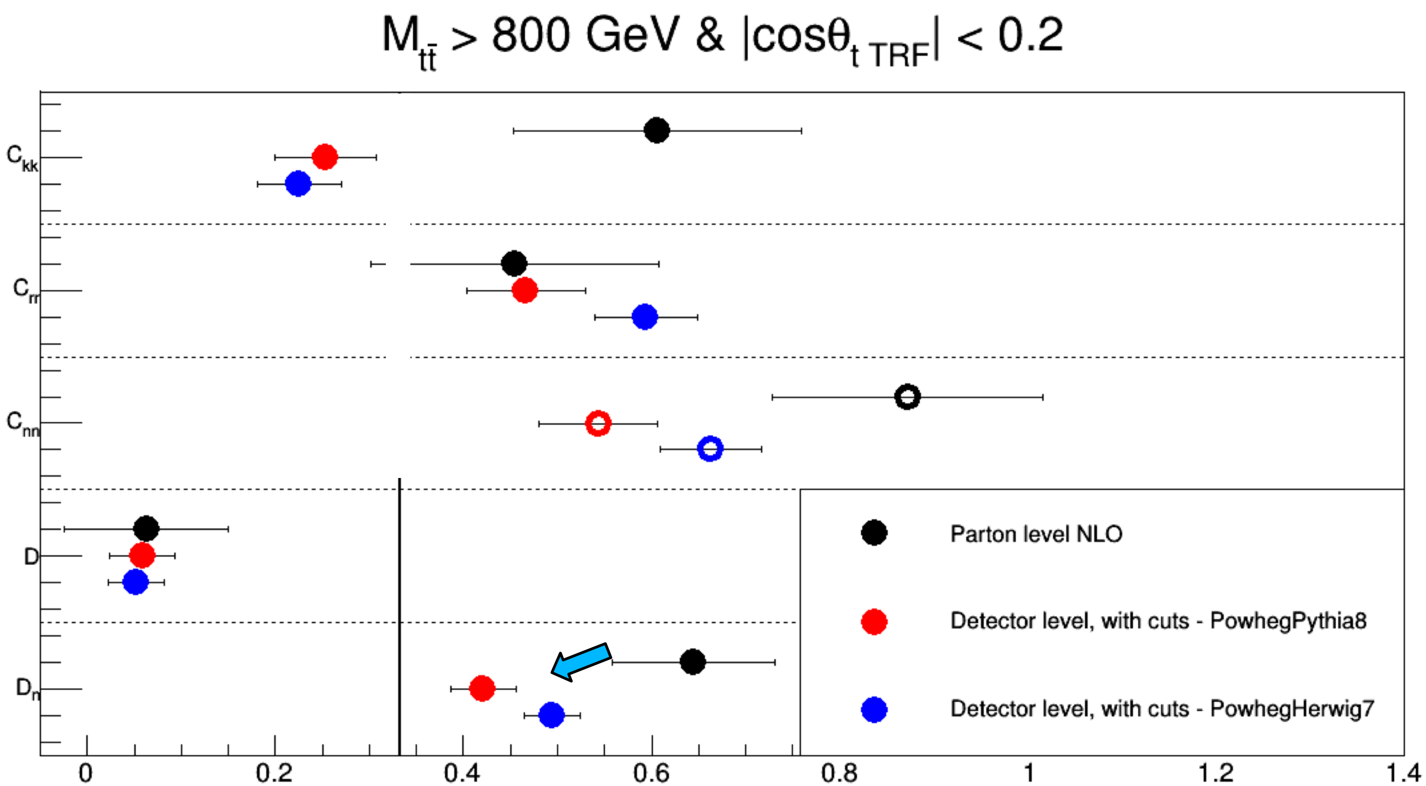

Migration effects: ~factor 1.5

using private ATLAS ntuples (thanks to Luis Monsonis); cuts on leptons and b-jets as well as top-quark reconstruction different to those used in the ATLAS published results

Note: Signs changed for Ci in the plot

	Parton-level	Detector-level	Migration factor
D – threshold regime	-0.54 ±0.02	-0.177 ±0.009	~3
Dn – boosted regime	0.64 ±0.09	0.42 ±0.03	~1.5

Sensitivity on SMEFT operators from those observables

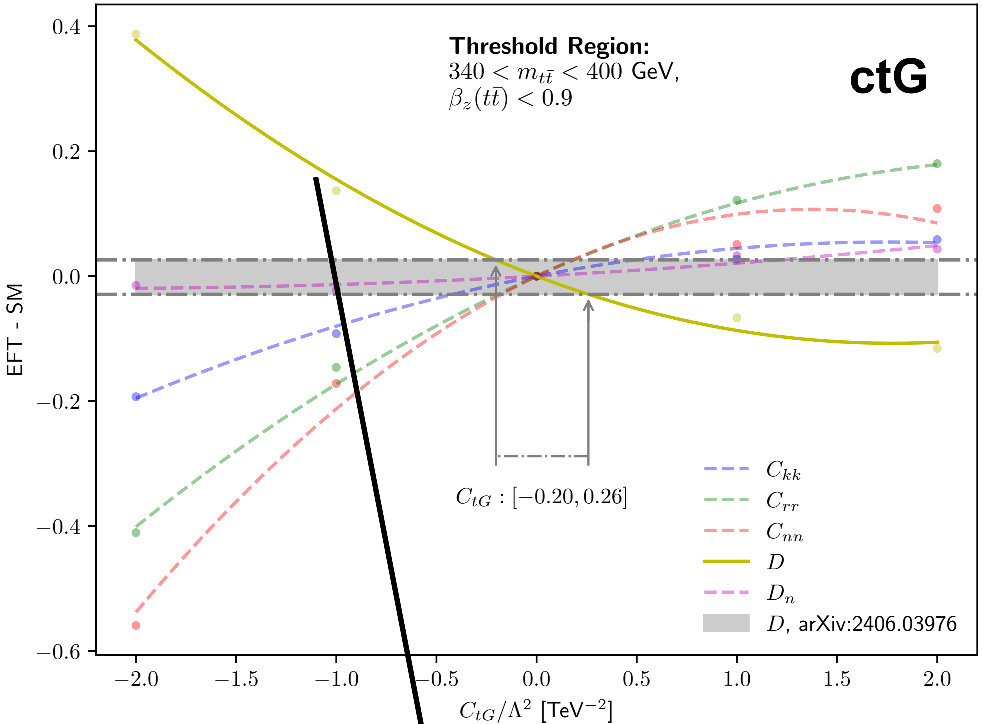

Adding scale unc.

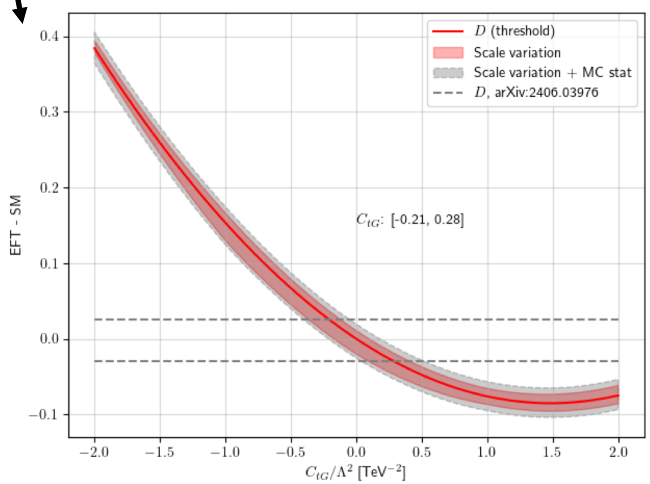

ctG limits from various observables @ boosted regime

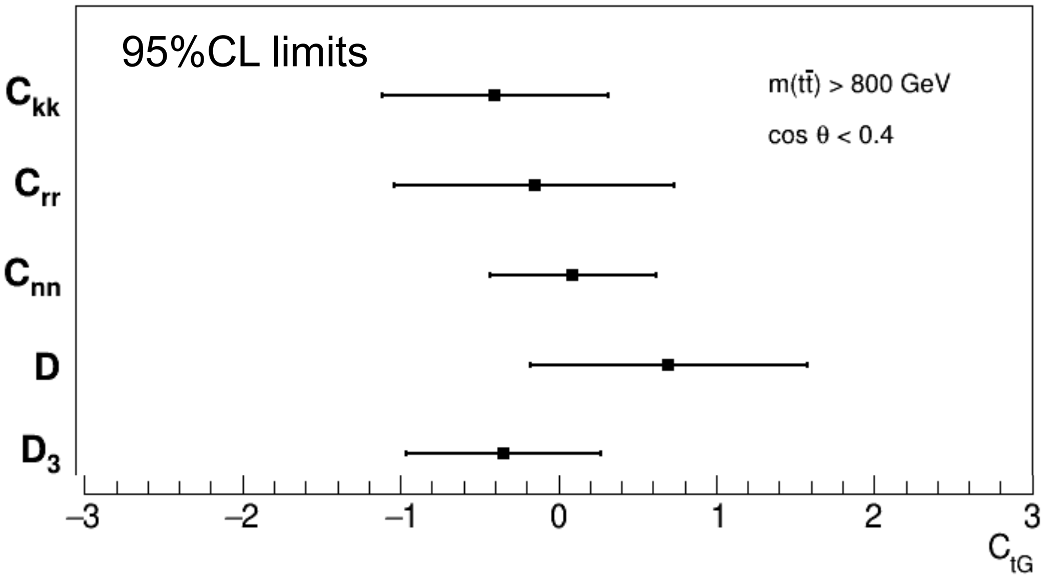

C_{tG} Const (2σ)	BOOSTED
Ckk	[-1.08,0.34]
Crr	[-1.00,0.76]
Cnn	[-0.40,0.64]
D	[-0.15,1.59]
D_3	[-0.93,0.30]

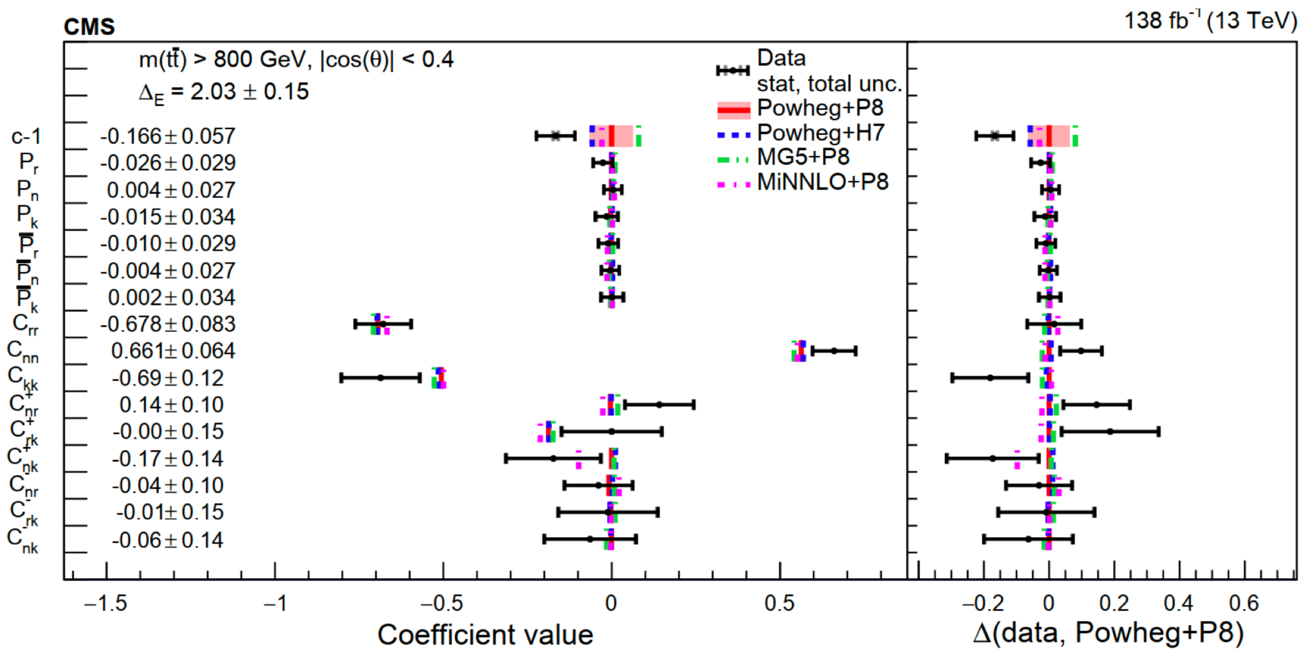

Limits from global fits with ~200 bins: [0.007,0.111]

arXiv:2105.00006

From CERN EP seminar, Giulia Negro (CMS)

Comparison with ATLAS

- **Entanglement in top quark observed by both ATLAS and CMS with >5 standard deviations!**
  - despite different analyses…

	ATLAS	CMS
Dataset	Full Run 2 (140 fb^{-1})	2016 (35.9 fb^{-1})
$t\bar{t}$ decay	Dilepton: eμ	Dilepton: ee, eμ and μμ
$t\bar{t}$ reconstruction	Ellipse method	Weighting method
Main selections	$340 < m(t\bar{t}) < 380$ GeV	$345 < m(t\bar{t}) < 400$ GeV, beta <0.9
Triggers	Single lepton	Single lepton + dilepton
Corrected to	Particle-level	Parton-level
Fit type	No fit, calibration curve	Profile likelihood template fit
Alternative hypothesis D	Reweighting	Mixing samples with/without spin corr
Threshold effects	Neglected	Considered (toponium contribution)
Nominal MC	PowhegBox+Pythia8	PowhegBox+Pythia8
Alternative MC	PowhegBox+Herwig7, bb4l	PowhegBox+Herwig++, MG5_AMC@NLO
Significance	**>> 5 standard deviations**	**> 5 standard deviations**

$$D_{obs} = -0.547 \pm 0.002(\text{stat}) \pm 0.021(\text{syst})$$
$$D_{exp} = -0.470 \pm 0.002(\text{stat}) \pm 0.018(\text{syst})$$

$$D_{obs} = -0.480^{+0.016}_{-0.017}(\text{stat})^{+0.020}_{-0.023}(\text{syst})$$
$$D_{exp} = -0.467^{+0.016}_{-0.017}(\text{stat})^{+0.021}_{-0.024}(\text{syst})$$

Top quark pair reconstruction

- Reconstruction of top quarks momenta complicated due to 2 neutrinos
  - Several methods were developed before, using m(top) and m(W) as constraints

NIM A 736 (2014) 169-178

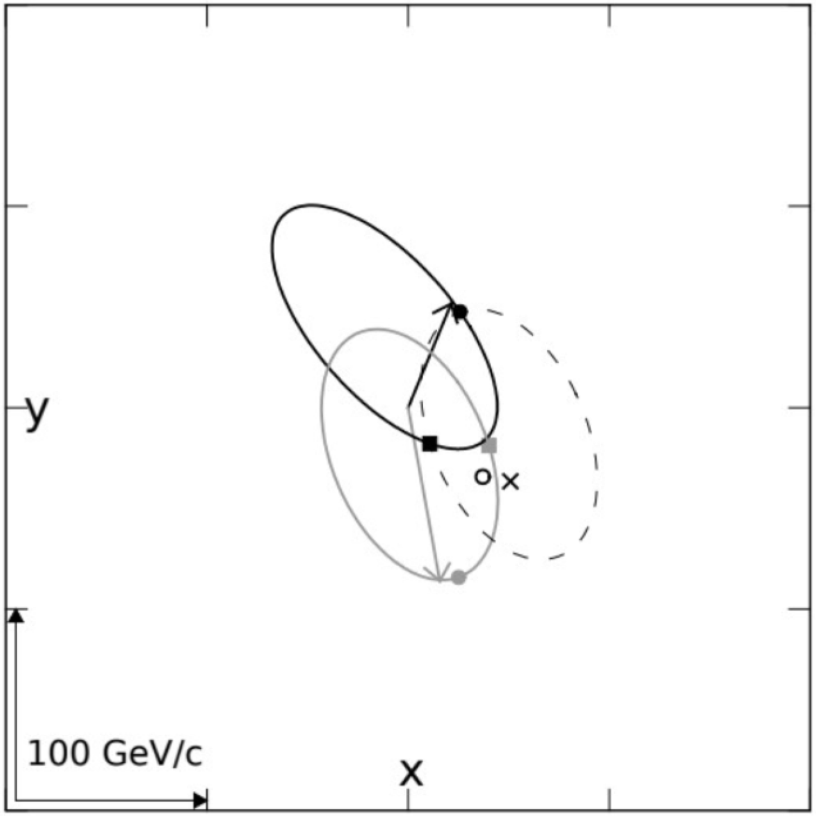

- A combination of various methods used:
  - Main method: **'Ellipse' method** (85% effic.)
    - Analytically calculate two ellipses for $p_T(\nu)$ and find intersections
  - If 'Ellipse' fails → **'Neutrino Weighting'** method (5%)
    - Scans $\eta(\nu)$, $\eta(\bar{\nu})$ phase-space
    - Solutions weighted based on compatibility between p_T of neutrinos and missing p_T
  - If both methods fail: **simple pairing** of leptons with the closest b-jets (10%)
    - Use highest-p_T jet if only 1 b-tagged jet

Dilepton vs lepton+jets top quark reconstruction

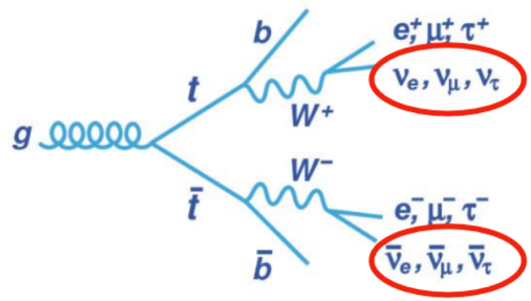

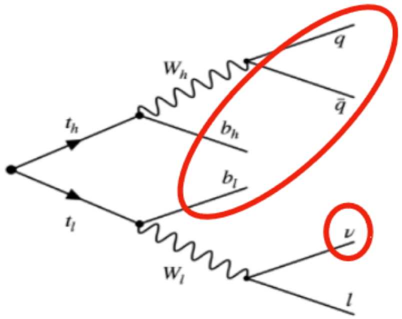

- $m_{\ell b}$ **weighting method**
  - use algebraic method to solve for neutrino 3-vectors
  - pick solution with smallest $m_{t\bar{t}}$
  - pair lepton and jet according to expected $m_{\ell b}$

$$
\begin{aligned}
\not{E}_x &= p_{\nu_x} + p_{\bar{\nu}_x} \\
\not{E}_y &= p_{\nu_y} + p_{\bar{\nu}_y}
\end{aligned}
$$

$$
\begin{aligned}
m_{W^+}^2 &= (E_{\ell^+} + E_\nu)^2 - (p_{\ell^+_x} + p_{\nu_x})^2, \\
&\quad -(p_{\ell^+_y} + p_{\nu_y})^2 - (p_{\ell^+_z} + p_{\nu_z})^2, \\
m_{W^-}^2 &= (E_{\ell^-} + E_{\bar{\nu}})^2 - (p_{\ell^-_x} + p_{\bar{\nu}_x})^2, \\
&\quad -(p_{\ell^-_y} + p_{\bar{\nu}_y})^2 - (p_{\ell^-_z} + p_{\bar{\nu}_z})^2, \\
m_t^2 &= (E_b + E_{\ell^+} + E_\nu)^2 - (p_{b_x} + p_{\ell^+_x} + p_{\nu_x})^2, \\
&\quad -(p_{b_y} + p_{\ell^+_y} + p_{\nu_y})^2 - (p_{b_z} + p_{\ell^+_z} + p_{\nu_z})^2, \\
m_{\bar{t}}^2 &= (E_{\bar{b}} + E_{\ell^-} + E_{\bar{\nu}})^2 - (p_{\bar{b}_x} + p_{\ell^-_x} + p_{\bar{\nu}_x})^2, \\
&\quad -(p_{\bar{b}_y} + p_{\ell^-_y} + p_{\bar{\nu}_y})^2 - (p_{\bar{b}_z} + p_{\ell^-_z} + p_{\bar{\nu}_z})^2
\end{aligned}
$$

- **Artificial NN**
  - goal = correctly identify detector-level objects and up/down jet assignment
  - NN trained on permutations
- For each event:
  - provide all possible permutations of objects as input to NN
  - use permutation resulting in the highest NN score
  - calculate neutrino momentum with W boson mass constraint

$$(p_\nu + p_l)^2 = m_W^2$$

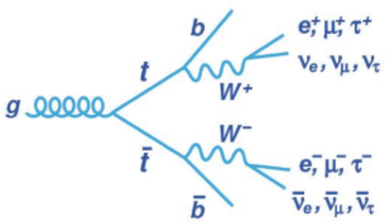

Dilepton vs lepton+jets

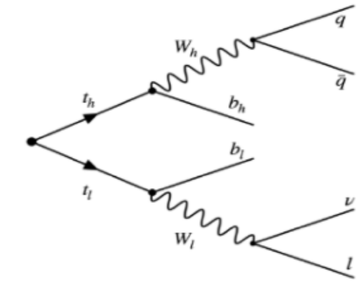

Dilepton

arXiv:2406.03976
accepted by ROPP

- **36.3 fb^{-1} of 2016 data @13 TeV**
  - based on PRD 100 (2019) 072002
- Lower branching ratio
- top spin info 100 % transmitted to charged leptons → easy to identify
- Lower p_T cuts for leading/subleading lepton (25/20 GeV) → higher efficiency at the threshold
- Worse $m_{t\bar{t}}$ resolution → not ideal for differential measurement
- Best for threshold region
  - high entanglement
  - mostly **time-like separated events**

Lepton + jets

arXiv:2409.11067
submitted to PRD

- **138 fb^{-1} of data @13 TeV** collected in **full Run 2**
- Higher branching ratio
- top spin info ~100 % transmitted to down-type quarks → hard to identify
- Higher p_T cut for single lepton (30 GeV) and for 4 jets (30 GeV) → lower efficiency at the threshold but OK for high $m_{t\bar{t}}$
- Better $m_{t\bar{t}}$ resolution → good for differential measurement
- Advantage for high $m_{t\bar{t}}$
  - high entanglement
  - mostly **space-like separated events**

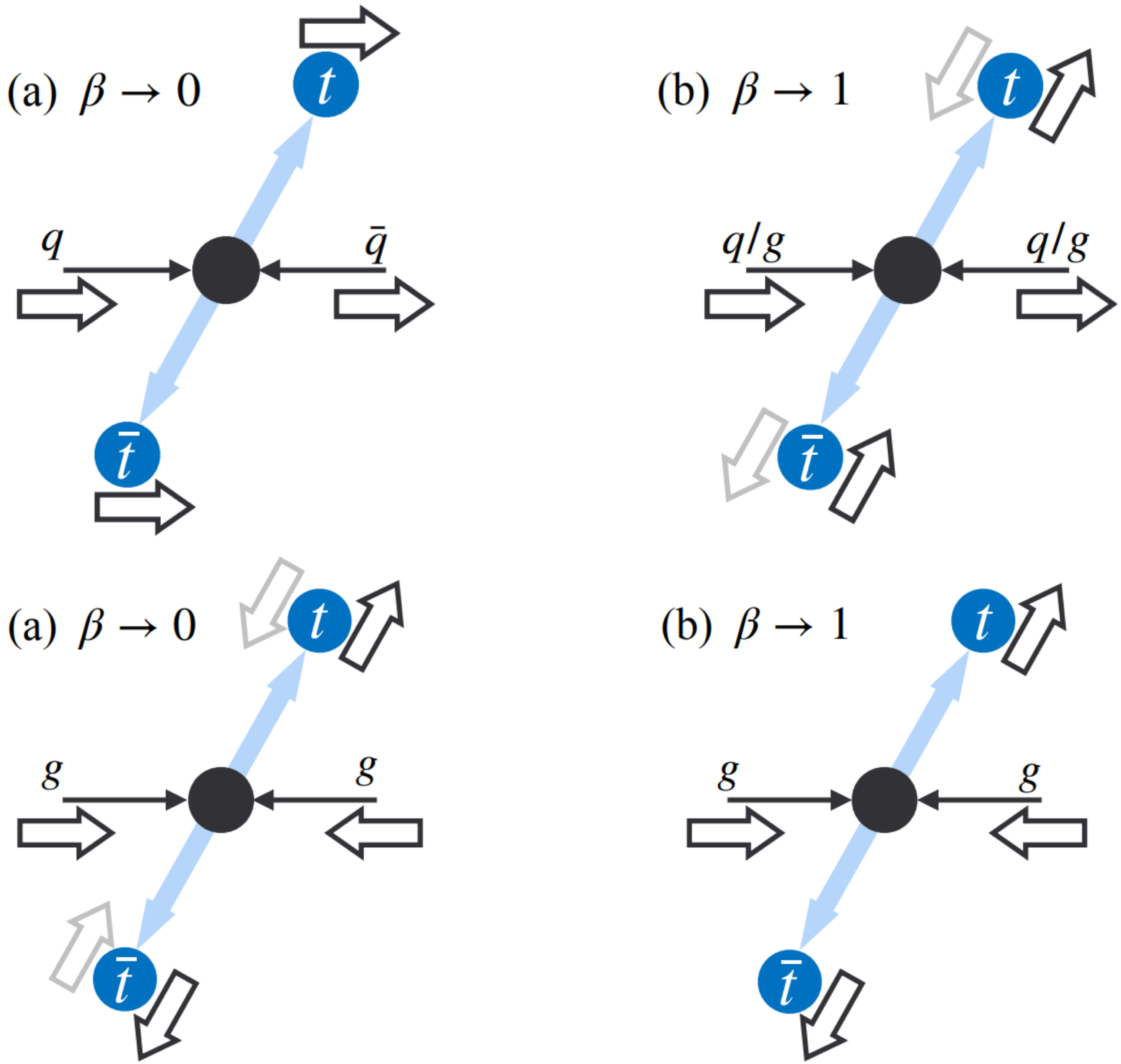
(a) $\beta \to 0$
t
q
$\bar{q}$
$\bar{t}$
(b) $\beta \to 1$
t
q/g
q/g
$\bar{t}$
(a) $\beta \to 0$
t
g
g
$\bar{t}$
(b) $\beta \to 1$
t
g
g
$\bar{t}$

EFT operators involving the top quark considered

8 two-fermion op.

Operator	Definition	Description
O_{tW}	$(\overline{Q}\sigma^{\mu\nu} t)\, \tau^I \tilde{\varphi} W^i_{\mu\nu}$	Modifies the tWb, $t\bar{t}\gamma$ and $t\bar{t}Z$ vertices
O_{tB}	$(\overline{Q}\sigma^{\mu\nu} t)\, \tilde{\varphi} B_{\mu\nu}$	Modifies the tWb, $t\bar{t}\gamma$ and $t\bar{t}Z$ vertices
O_{tG}	$(\overline{Q}\sigma^{\mu\nu} T^a t)\, \tilde{\varphi} G^a_{\mu\nu}$	Modifies the $t\bar{t}g$ vertex
$O^{(1)}_{\varphi Q}$	$\left(\varphi^\dagger i \overleftrightarrow{D}_\mu \varphi\right) (\overline{Q}\gamma^\mu Q)$	Modifies the $b\bar{b}Z$ and $t\bar{t}Z$ vertices
$O^{(3)}_{\varphi Q}$	$\left(\varphi^\dagger i \overleftrightarrow{D}^i_\mu \varphi\right) (\overline{Q}\tau^I \gamma^\mu Q)$	Modifies the tWb, $b\bar{b}Z$ and $t\bar{t}Z$ vertices
$O_{\varphi t}$	$\left(\varphi^\dagger i \overleftrightarrow{D}_\mu \varphi\right) (\bar{t}\gamma^\mu t)$	Modifies the $t\bar{t}Z$ vertex
$O_{t\varphi}$	$(\overline{Q}t)\, (\epsilon \varphi^* \varphi^\dagger \varphi)$	Modifies Yukawa coupling of the top quarks
$O_{\varphi b}$	$\left(\varphi^\dagger i \overleftrightarrow{D}_\mu \varphi\right) (\bar{b}\gamma^\mu b)$	Modifies the $b\bar{b}Z$ vertex

14 four-fermion op.

$q_i = (u^i_L, d^i_L)$	$u_i = u^i_R,\ d_i = d^i_R$	$i = 1, 2$
$Q = (t_L, b_L)$	$t = t_R,\ b = b_R$	

- 8 four-quark operators with LL and RR chiral structure

$$O^{1,8}_{Qq} = (\bar{Q}\gamma_\mu T^A Q)(\bar{q}_i \gamma^\mu T^A q_i) \qquad O^{1,1}_{Qq} = (\bar{Q}\gamma_\mu Q)(\bar{q}_i \gamma^\mu q_i)$$
$$O^{3,8}_{Qq} = (\bar{Q}\gamma_\mu T^A \tau^I Q)(\bar{q}_i \gamma^\mu T^A \tau^I q_i) \qquad O^{3,1}_{Qq} = (\bar{Q}\gamma_\mu \tau^I Q)(\bar{q}_i \gamma^\mu \tau^I q_i)$$
$$O^{8}_{tu} = (\bar{t}\gamma_\mu T^A t)(\bar{u}_i \gamma^\mu T^A u_i) \qquad O^{1}_{tu} = (\bar{t}\gamma_\mu t)(\bar{u}_i \gamma^\mu u_i)$$
$$O^{8}_{td} = (\bar{t}\gamma^\mu T^A t)(\bar{d}_i \gamma_\mu T^A d_i) \qquad O^{1}_{td} = (\bar{t}\gamma^\mu t)(\bar{d}_i \gamma_\mu d_i)\ ;$$

- 6 four-quark operators with LR and RL chiral structure

$$O^{8}_{Qu} = (\bar{Q}\gamma^\mu T^A Q)(\bar{u}_i \gamma_\mu T^A u_i) \qquad O^{1}_{Qu} = (\bar{Q}\gamma^\mu Q)(\bar{u}_i \gamma_\mu u_i)$$
$$O^{8}_{Qd} = (\bar{Q}\gamma^\mu T^A Q)(\bar{d}_i \gamma_\mu T^A d_i) \qquad O^{1}_{Qd} = (\bar{Q}\gamma^\mu Q)(\bar{d}_i \gamma_\mu d_i)$$
$$O^{8}_{tq} = (\bar{q}_i \gamma^\mu T^A q_i)(\bar{t}\gamma_\mu T^A t) \qquad O^{1}_{tq} = (\bar{q}_i \gamma^\mu q_i)(\bar{t}\gamma_\mu t)\ ;$$

JHEP02(2020)131

SMEFT operators relevant for the top quark

Basis: complete, non-redundant set of operators
Dimension 6: several operators affecting top quark interactions

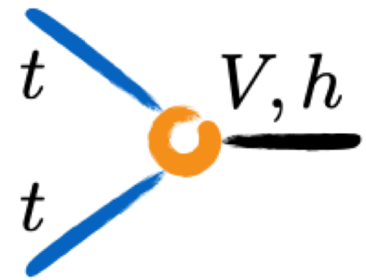

Two-fermion op. (2F): QQ + V,G,φ

Four-fermion op. (4F): QQQQ, QQqq, QQll

- The exact number depends on CP/flavour assumptions
- In our studies, we consider only real parameters
- In our first study, we considered eight 2F operators

Left and right-handed couplings of the t- and b-quark to the Z

$$O^{3}_{\varphi Q} \equiv \tfrac{1}{2}(\bar{q}\tau^{I}\gamma^{\mu}q)\left(\varphi^{\dagger} i \overleftrightarrow{D}^{I}_{\mu}\varphi\right)$$
$$O^{1}_{\varphi Q} \equiv \tfrac{1}{2}(\bar{q}\gamma^{\mu}q)\left(\varphi^{\dagger} i \overleftrightarrow{D}_{\mu}\varphi\right)$$
$$O_{\varphi u} \equiv \tfrac{1}{2}(\bar{u}\gamma^{\mu}u)\left(\varphi^{\dagger} i \overleftrightarrow{D}_{\mu}\varphi\right)$$
$$\cancel{O_{\varphi d} \equiv \tfrac{1}{2}(\bar{d}\gamma^{\mu}d)\left(\varphi^{\dagger} i \overleftrightarrow{D}_{\mu}\varphi\right)}$$

vector

EW dipole operators

$$O_{uW} \equiv (\bar{q}\tau^{I}\sigma^{\mu\nu}u)\left(\varepsilon\varphi^{*}W^{I}_{\mu\nu}\right)$$
$$O_{dW} \equiv (\bar{q}\tau^{I}\sigma^{\mu\nu}d)\left(\varphi W^{I}_{\mu\nu}\right)$$
$$O_{uB} \equiv (\bar{q}\sigma^{\mu\nu}u)(\varepsilon\varphi^{*}B_{\mu\nu})$$
$$\cancel{O_{dB} \equiv (\bar{q}\sigma^{\mu\nu}d)(\varphi B_{\mu\nu})}$$

tensor

Chromo magnetic dipole operators

$$O_{uG} \equiv (\bar{q}\sigma^{\mu\nu}T^{A}u)\left(\varepsilon\varphi^{*}G^{A}_{\mu\nu}\right)$$
$$O_{dG} \equiv (\bar{q}\sigma^{\mu\nu}T^{A}d)\left(\varphi G^{A}_{\mu\nu}\right)$$

tensor

Top/Bottom yukawa

$$O_{u\varphi} \equiv (\bar{q}u)(\varepsilon\varphi^{*}\,\varphi^{\dagger}\varphi)$$
$$O_{d\varphi} \equiv (\bar{q}d)(\varphi\,\varphi^{\dagger}\varphi)$$

scalar

Charged current interaction

$$O_{\varphi ud} \equiv \tfrac{1}{2}(\bar{u}\gamma^{\mu}d)(\varphi^{T}\varepsilon i D_{\mu}\varphi)$$

vector

2F operators relevant for top quark physics

$\mathcal{O}_{tW}, \mathcal{O}_{tB}$ - $t\bar{t}Z$ and $t\bar{t}\gamma$ vertices

$\mathcal{O}_{\phi t}, \mathcal{O}_{\phi Q^{3}}, \mathcal{O}_{\phi Q^{1}}$ - $t\bar{t}Z$ vertex

Basis rotated following the prescription of the LHC Top WG:
$O_{tB} \rightarrow O_{tZ} = \cos\theta_{W} O_{tW} - \sin\theta_{W} O_{tB}$
$O^{(1)}_{\varphi Q} \rightarrow O_{\varphi Q} = O^{(1)}_{\varphi Q} - O^{(3)}_{\varphi Q}$

arXiv: 1802.07237

Measurements used in our fit to top quark EW couplings

JHEP02(2022)032

Process	Observable	$\sqrt{s}$	$\int \mathcal{L}$	Experiment
$pp \to t\bar{t}H + tHq$	σ	13 TeV	140 fb^{-1}	ATLAS
$pp \to t\bar{t}Z$	$d\sigma/dp_T^Z$ (7 bins)	13 TeV	140 fb^{-1}	ATLAS
$pp \to t\bar{t}\gamma$	$d\sigma/dp_T^\gamma$ (11 bins)	13 TeV	140 fb^{-1}	ATLAS
$pp \to tZq$	σ	13 TeV	77.4 fb^{-1}	CMS
$pp \to t\gamma q$	σ	13 TeV	36 fb^{-1}	CMS
$pp \to t\bar{t}W$	σ	13 TeV	36 fb^{-1}	CMS
$pp \to t\bar{b}$ (s-ch)	σ	8 TeV	20 fb^{-1}	LHC
$pp \to tW$	σ	8 TeV	20 fb^{-1}	LHC
$pp \to tq$ (t-ch)	σ	8 TeV	20 fb^{-1}	LHC
$t \to Wb$	$F_0,\ F_L$	8 TeV	20 fb^{-1}	LHC
$p\bar{p} \to t\bar{b}$ (s-ch)	σ	1.96 TeV	9.7 fb^{-1}	Tevatron
$e^-e^+ \to b\bar{b}$	R_b , A_{FBLR}^{bb}	$\sim$ 91 GeV	202.1 pb^{-1}	LEP/SLD

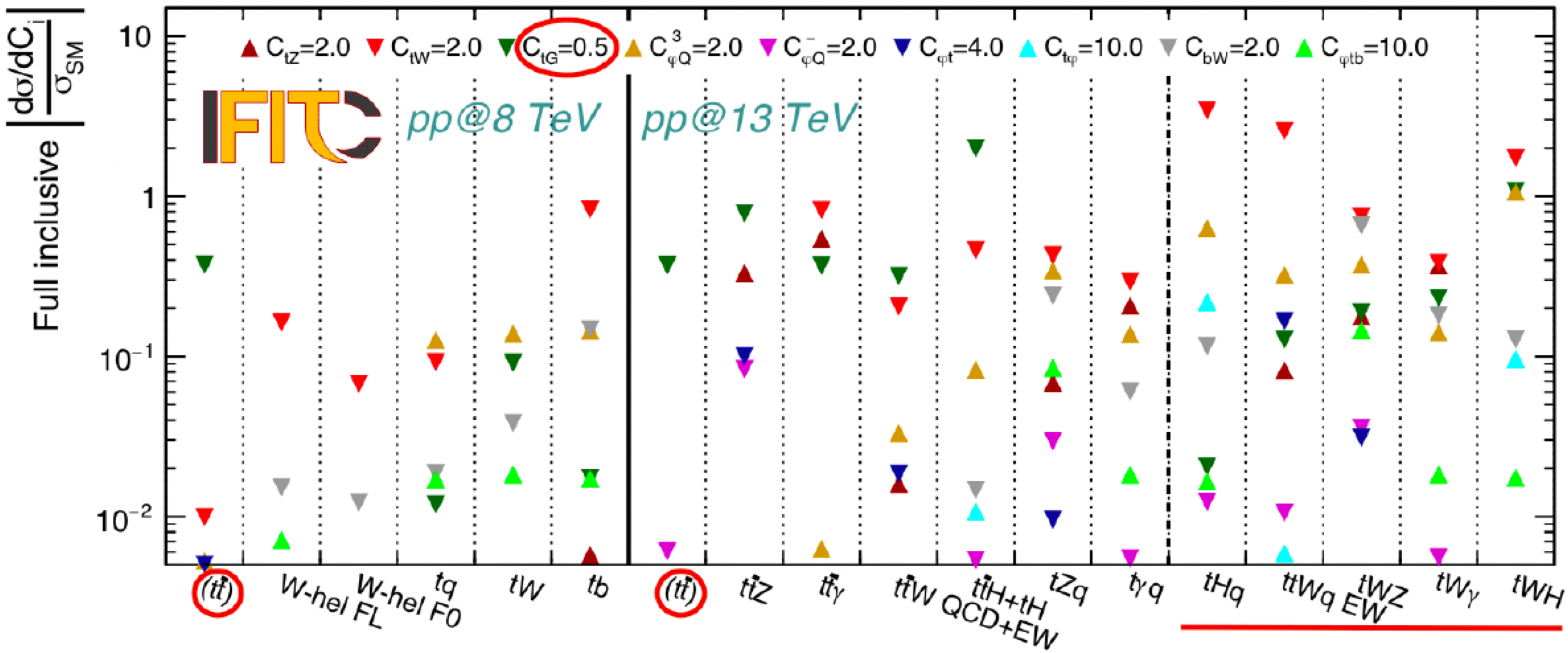
Full inclusive $\left|\frac{d\sigma/dC_i}{\sigma_{SM}}\right|$
10
1
10^{-1}
10^{-2}
C_{tZ}=2.0 C_{tW}=2.0 C_{tG}=0.5 $C^3_{\varphi Q}$=2.0 $C^-_{\varphi Q}$=2.0 $C_{\varphi t}$=4.0 $C_{t\varphi}$=10.0 C_{bW}=2.0 $C_{\varphi tb}$=10.0
IFIC
pp@8 TeV
pp@13 TeV
(tt̄)
W-hel FL
W-hel F0
tq
tW
tb
(tt̄)
tt̄Z
tt̄γ
tt̄W
tt̄H+tH QCD+EW
tZq
tγq
tHq
ttWq EW
tWZ
tWγ
tWH

Sensitivity of each observable

* LH/RH couplings of t/b quarks to Z: $O_{\varphi t}, O^{-}_{\varphi Q}, O^{(3)}_{\varphi Q}$
* EW dipole operators: O_{tZ}, O_{tW}, O_{bW}
* Top Yukawa: $O_{t\varphi}$
* Charged current interaction: $O_{\varphi tb}$

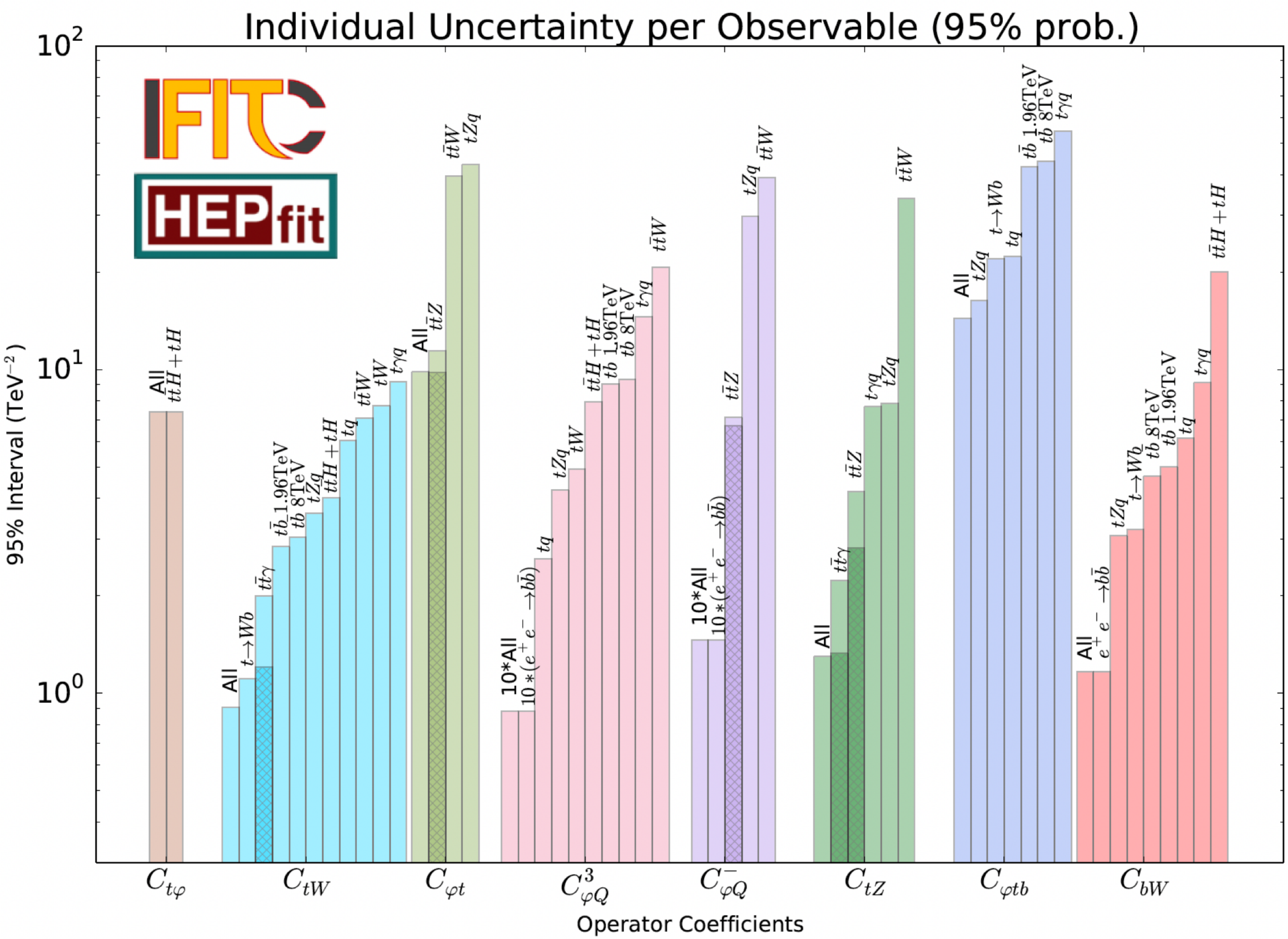

Purple and green bars
Dark: differential $t\bar{t}Z$ and $t\bar{t}\gamma$
Light (full length): inclusive "

Sensitivity coming from:
C_{tW} → W helicity and $t\bar{t}\gamma$
$C_{\varphi t}$ → $t\bar{t}Z$
$C^{-}_{\varphi Q}$ & $C^{(3)}_{\varphi Q}$ → LEP/SLC
C_{tZ} → $t\bar{t}\gamma$ and $t\bar{t}Z$
$C_{\varphi tb}$ → tZ and W helicity

Significant improvement from $t\bar{t}Z$ and $t\bar{t}\gamma$ differential measurements ☺

JHEP02(2022)032

Complementarity between observables

* LH/RH couplings of t/b quarks to Z: $O_{\varphi t}, O^{-}_{\varphi Q}, O^{(3)}_{\varphi Q}$

* EW dipole operators: O_{tZ}, O_{tW}, O_{bW}

* Top Yukawa: $O_{t\varphi}$

* Charged current interaction: $O_{\varphi tb}$

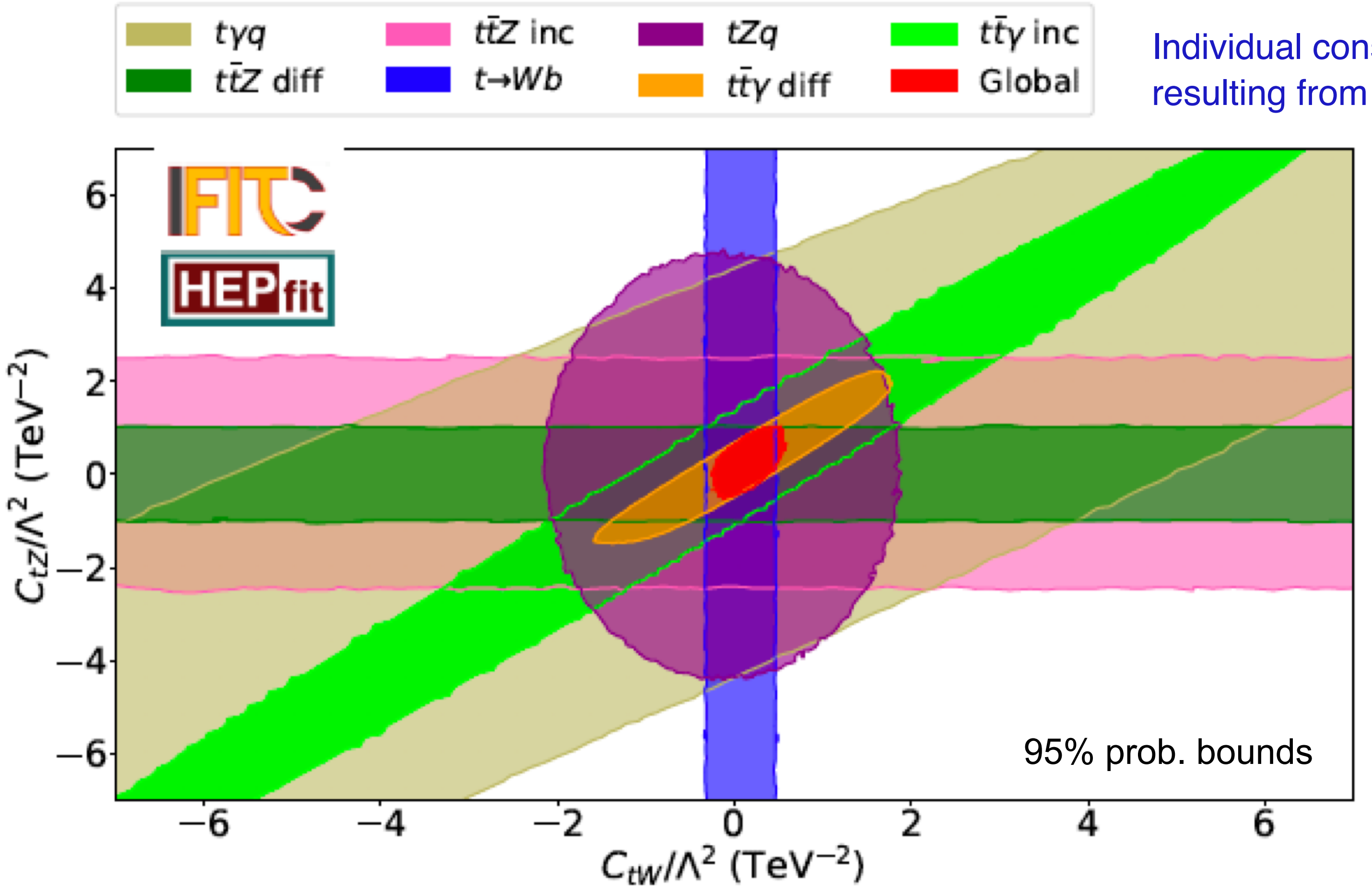

Individual constraints on the eight Wilson coefficient resulting from measurements in different processes

Sensitivity coming from:

C_{tW} → W helicity and $t\bar{t}\gamma$

C_{tZ} → $t\bar{t}\gamma$ and $t\bar{t}Z$

Significant improvement from $t\bar{t}Z$ and $t\bar{t}\gamma$ differential measurements ☺

JHEP02(2022)032

Results of the global fit

✓ Constraints of **linear** (only Λ^{-2} terms) global fit are similar to those of the **quadratic** (Λ^{-2}+Λ^{-4}) fit
- Overall comparable results
- Main difference between the two sets of results seen for $\boldsymbol{C_{tZ}}$

✓ Bounds compatible with SM within 2σ
✓ 95% prob. bounds: $\pm$ 0.35-7 TeV^{-2}

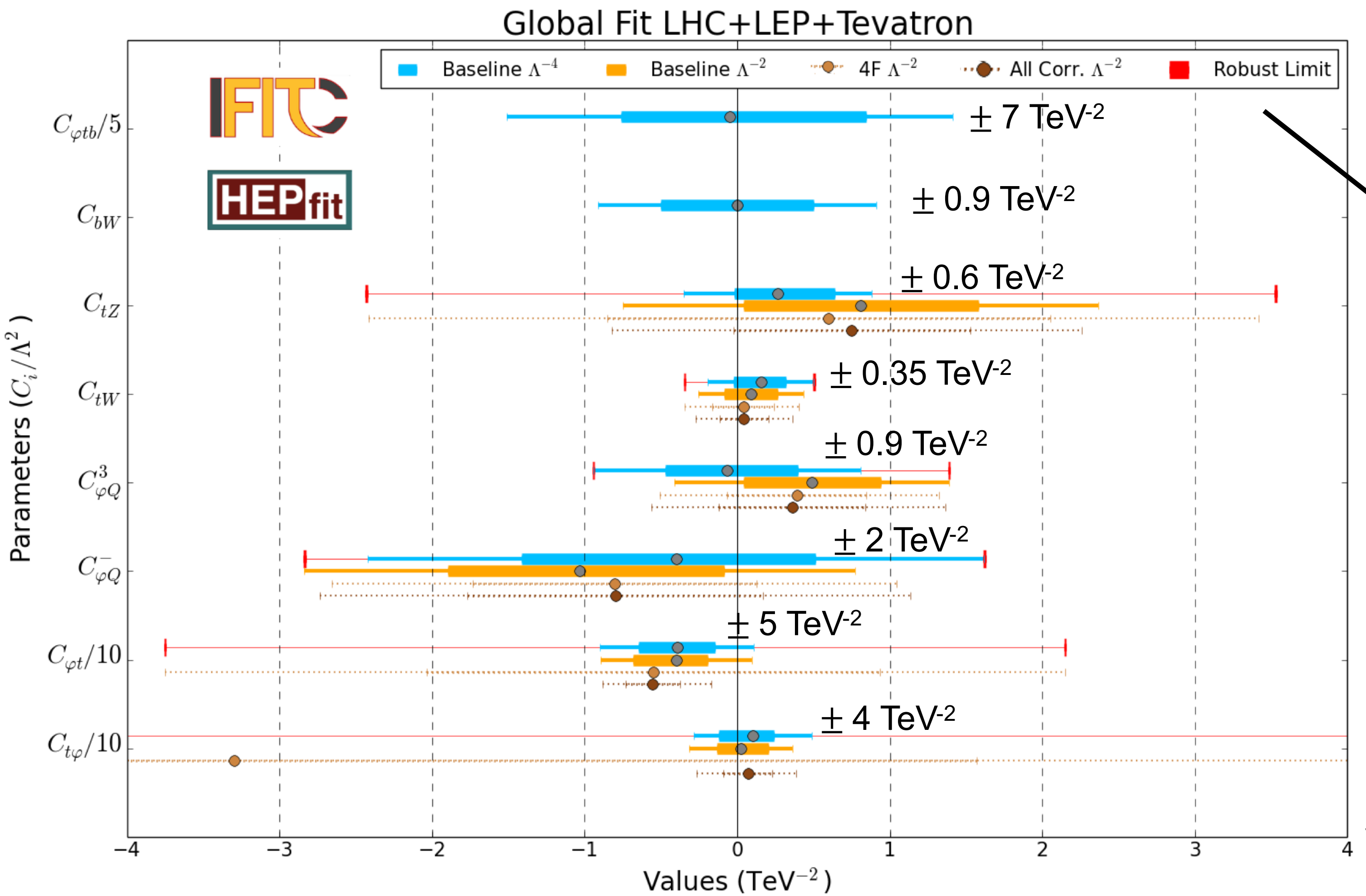

Check the robustness of the fit:

1) Extension of our basis: with seven 4F QQqq operators and C_{tG}

2) Correlations between different observables (ansatzs for non-published correlations have been estimated)

3) Missing higher-orders in α_S in EFT parametrisations

→ **Robust limits:** envelope obtained from results of new fits with these effects

JHEP02(2022)032

Including more observables and extending the basis

Including observables sensitive to 4F, the robust limits improve.

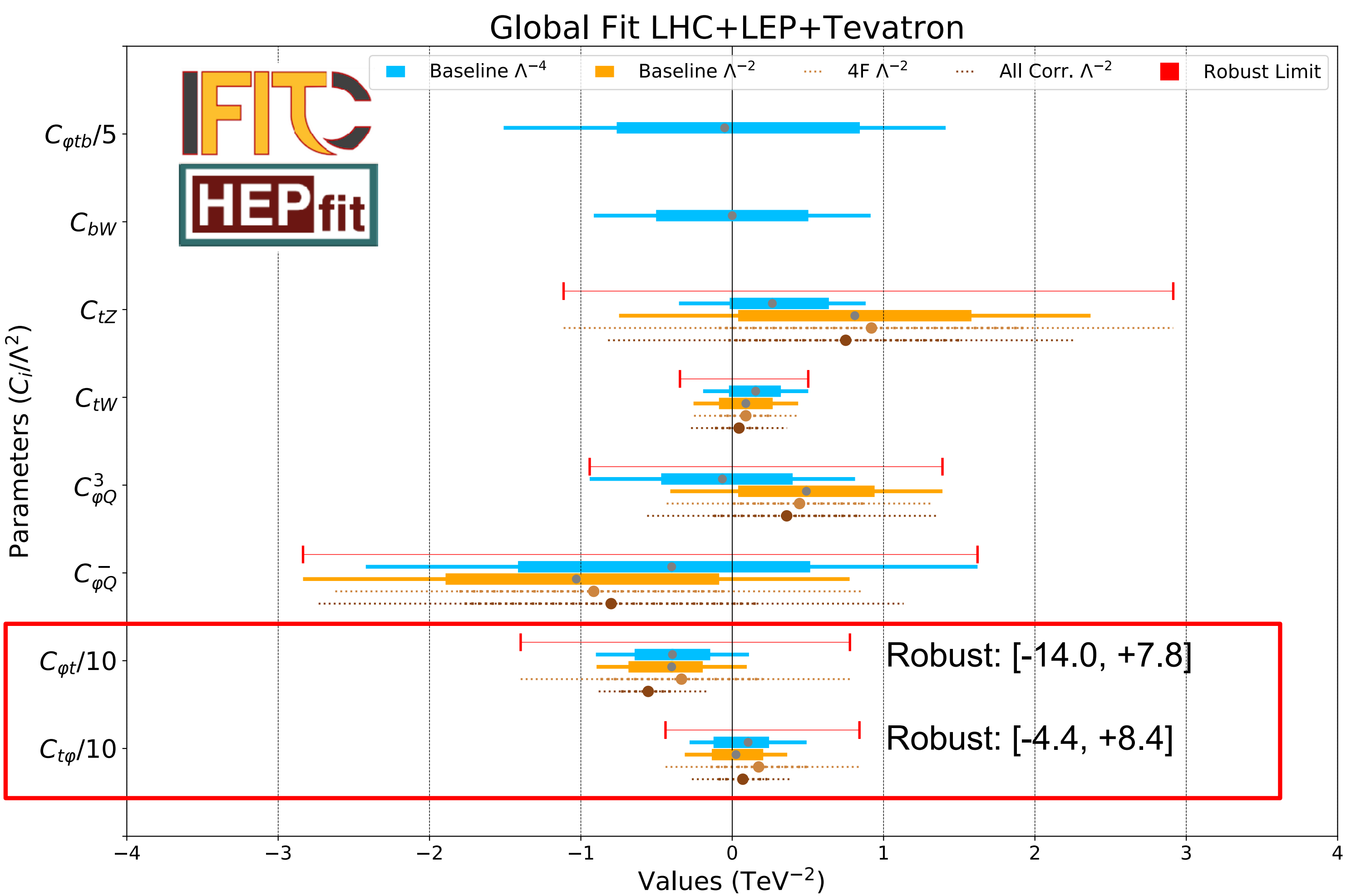

Including :

- observables: diff. *tt* XS and A_c
- some 4F operators: QQqq
- linear terms only

95% CL bounds

C/Λ^2 (TeV^{-2})	Linear (95% probability) Individual	Linear (95% probability) Global-Baseline	Lin.+Quad. (95% probability) Individual	Lin.+Quad. (95% probability) Global-Baseline	(95% probability) Global-Robust
$C_{t\varphi}$	[-3.17, 3.47]	[-3.13, 3.63]	[-3.05, 4.05]	[-2.82, 4.92]	[-121.82, 62.82]
$C_{\varphi Q}^{-}$	[-0.038, 0.079]	[-2.84, 0.78]	[-0.038, 0.079]	[-2.42, 1.62]	[-2.84, 1.62]
$C_{\varphi Q}^{3}$	[-0.019, 0.040]	[-0.41, 1.39]	[-0.019, 0.040]	[-0.94, 0.81]	[-0.94, 1.39]
$C_{\varphi t}$	[-6.6, 1.8]	[-8.96, 0.96]	[-8.6, 1.5]	[-9.01, 1.11]	[-37.50, 21.50]
C_{tW}	[-0.30, 0.38]	[-0.26, 0.44]	[-0.28, 0.32]	[-0.19, 0.50]	[-0.35, 0.50]
C_{tZ}	[-0.82, 2.21]	[-0.75, 2.37]	[-0.39, 0.57]	[-0.35, 0.88]	[-2.43, 3.53]
$C_{\varphi tb}$	–	–	[-6.61, 6.71]	[-7.55, 7.05]	–
C_{bW}	–	–	[-0.47, 0.47]	[-0.91, 0.91]	–

The power of differential cross sections

JHEP 09 (2020) 049

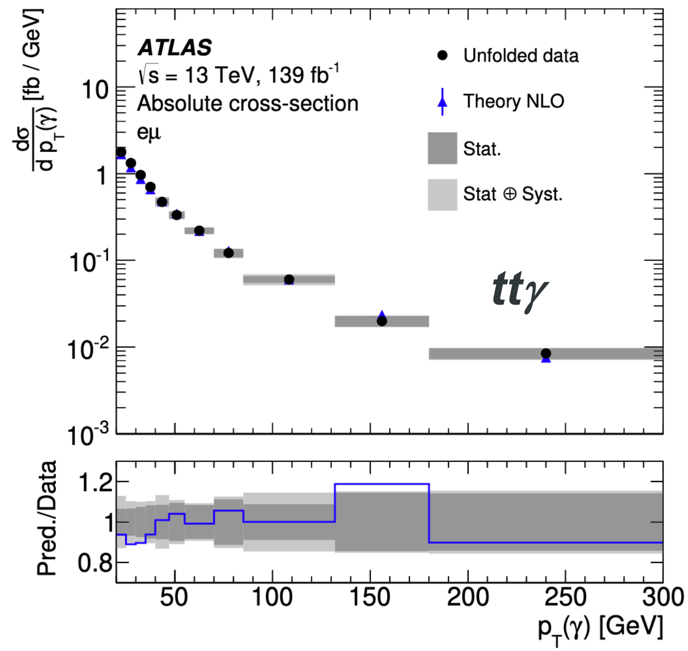

Eur. Phys. J. C 81 (2021) 737

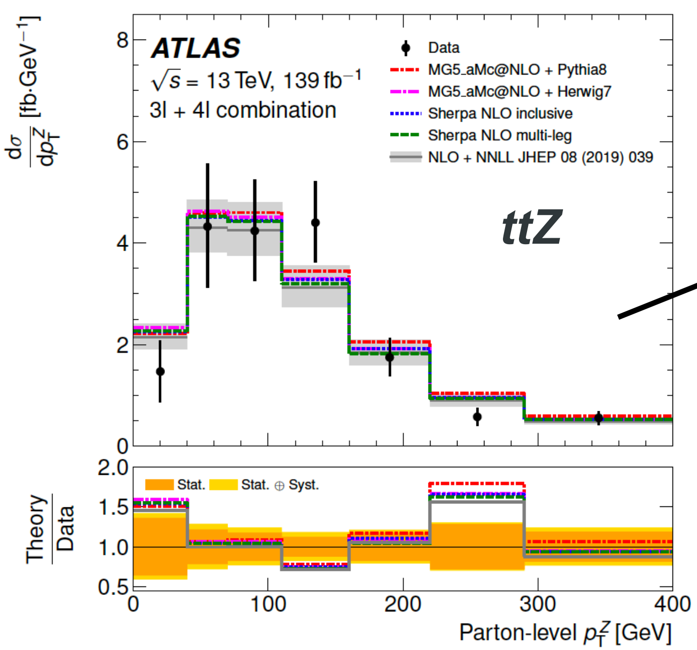

Dependence derived with **MadGraph5_aMC@NLO**, plus **SMEFT@NLO** and **TEFT_EW**

$$X = X_{\mathrm{SM}} + \underbrace{\boxed{\frac{1}{\Lambda^2}\sum_i C_i X_i^{(1)}}}_{\text{Linear Terms}} + \underbrace{\boxed{\frac{1}{\Lambda^4}\sum_{ij} C_i C_j X_{ij}^{(2)}}}_{\text{Quadratic Terms}} + \mathcal{O}(\Lambda^{-4})$$

JHEP02(2022)032

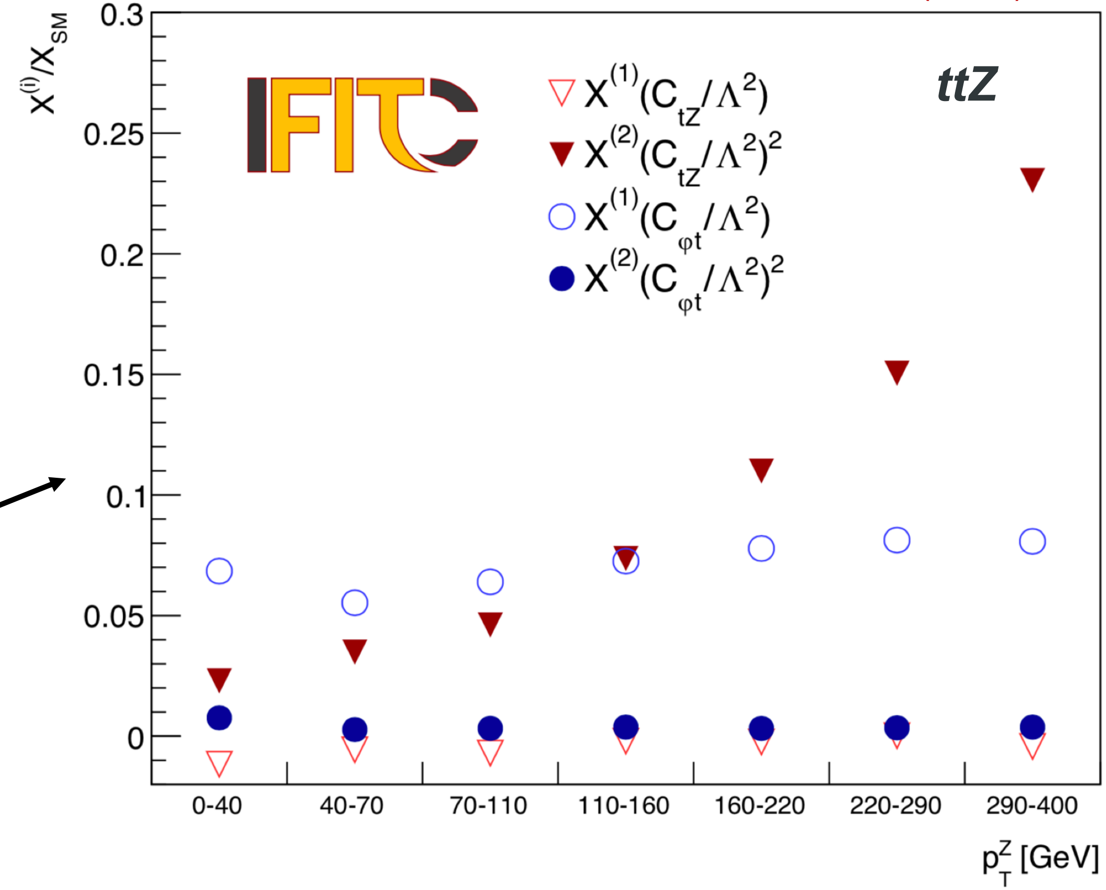

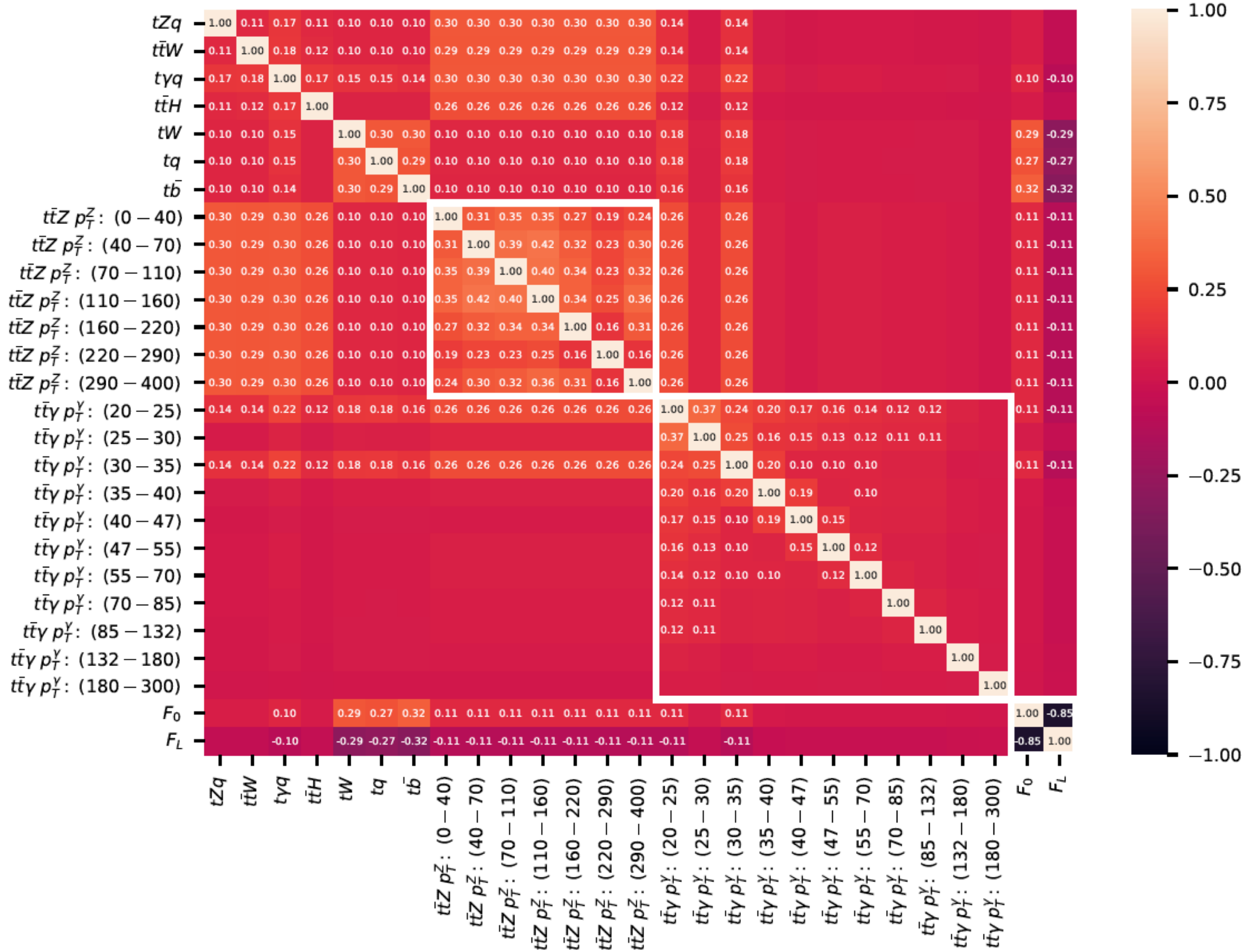
tZq
$t\bar{t}W$
$t\gamma q$
$t\bar{t}H$
tW
tq
$t\bar{b}$
$t\bar{t}Z\ p_T^Z$: (0 − 40)
$t\bar{t}Z\ p_T^Z$: (40 − 70)
$t\bar{t}Z\ p_T^Z$: (70 − 110)
$t\bar{t}Z\ p_T^Z$: (110 − 160)
$t\bar{t}Z\ p_T^Z$: (160 − 220)
$t\bar{t}Z\ p_T^Z$: (220 − 290)
$t\bar{t}Z\ p_T^Z$: (290 − 400)
$t\bar{t}\gamma\ p_T^\gamma$: (20 − 25)
$t\bar{t}\gamma\ p_T^\gamma$: (25 − 30)
$t\bar{t}\gamma\ p_T^\gamma$: (30 − 35)
$t\bar{t}\gamma\ p_T^\gamma$: (35 − 40)
$t\bar{t}\gamma\ p_T^\gamma$: (40 − 47)
$t\bar{t}\gamma\ p_T^\gamma$: (47 − 55)
$t\bar{t}\gamma\ p_T^\gamma$: (55 − 70)
$t\bar{t}\gamma\ p_T^\gamma$: (70 − 85)
$t\bar{t}\gamma\ p_T^\gamma$: (85 − 132)
$t\bar{t}\gamma\ p_T^\gamma$: (132 − 180)
$t\bar{t}\gamma\ p_T^\gamma$: (180 − 300)
F_0
F_L
1.00
0.75
0.50
0.25
0.00
−0.25
−0.50
−0.75
−1.00

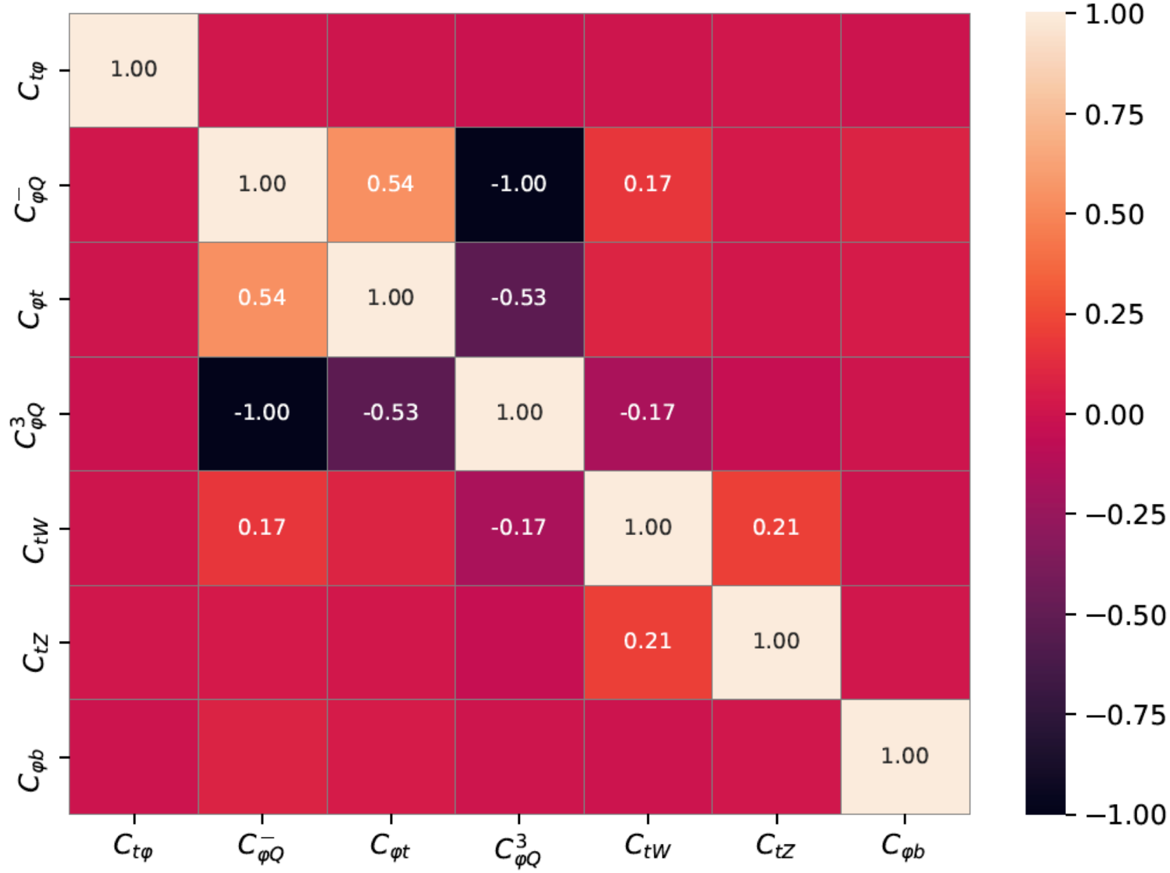

Figure A.3: Correlation matrix between the different EFT operators obtained in the baseline linear (Λ^{-2}) fit. Cells are filled if the correlation is higher than 10% in absolute value. The operator $O_{\varphi b}$, that modifies only the bottom quark electro-weak couplings, is taken into account in the fit but limits on its coefficients are not reported since the obtained values are not competitive using only the observables considered in the fit.

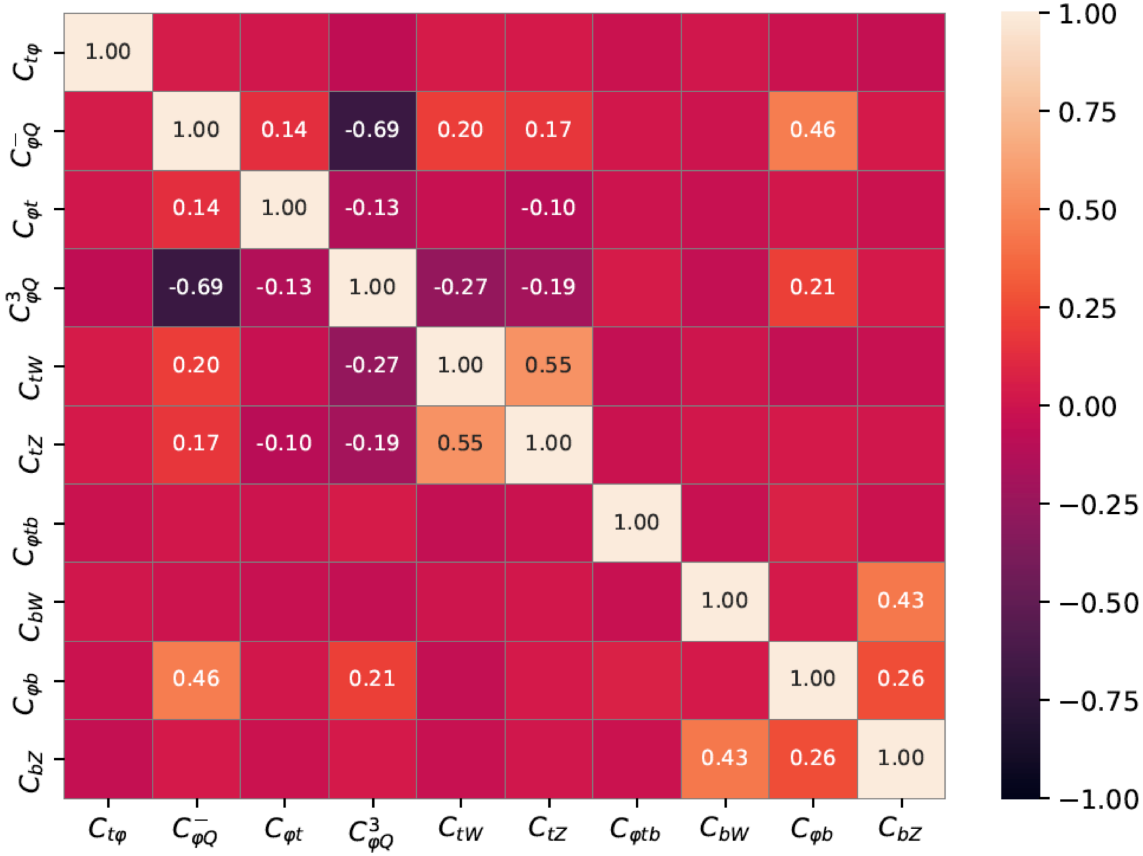

Figure A.4: Correlation matrix between the different EFT operators obtained in the baseline quadratic (Λ^{-4}) fit. Cells are filled if the correlation is higher than 10% in absolute value. The operators that modify only the bottom quark electroweak couplings, $O_{\varphi d}$ and O_{dZ}, are taken into account in the fit but limits on their coefficients are not reported since the obtained values are not competitive using only the observables considered in the fit.

4F operators: experimental constraints from tt production

- ATLAS has put tight limits on these 4-fermion operators

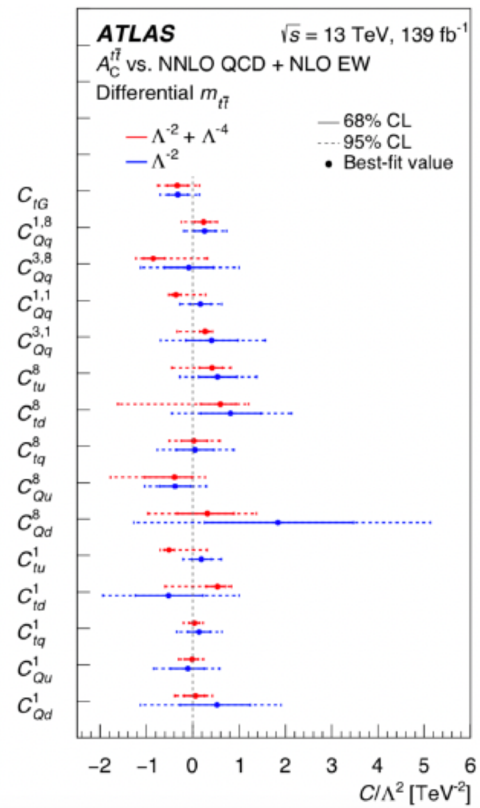

Evidence for the charge asymmetry in $pp \to t\bar{t}$ production at $\sqrt{s} = 13$ TeV with the ATLAS detector [arXiv:2208.12095]

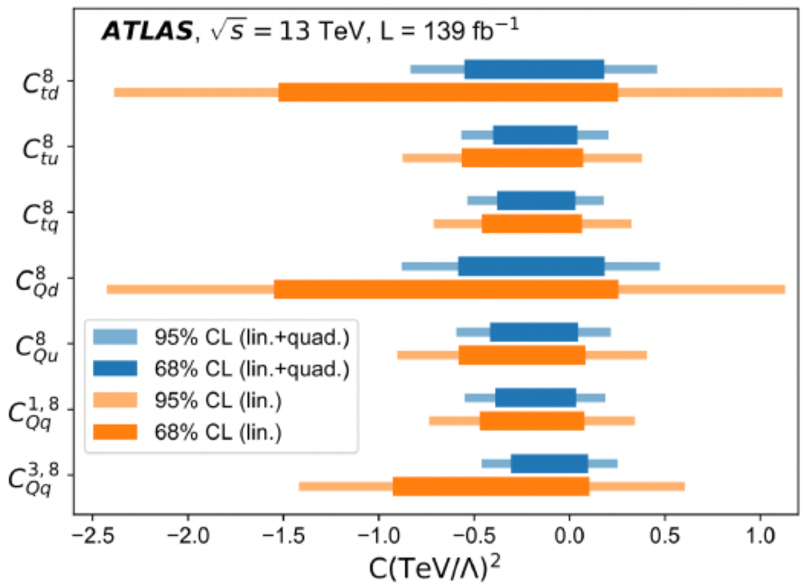

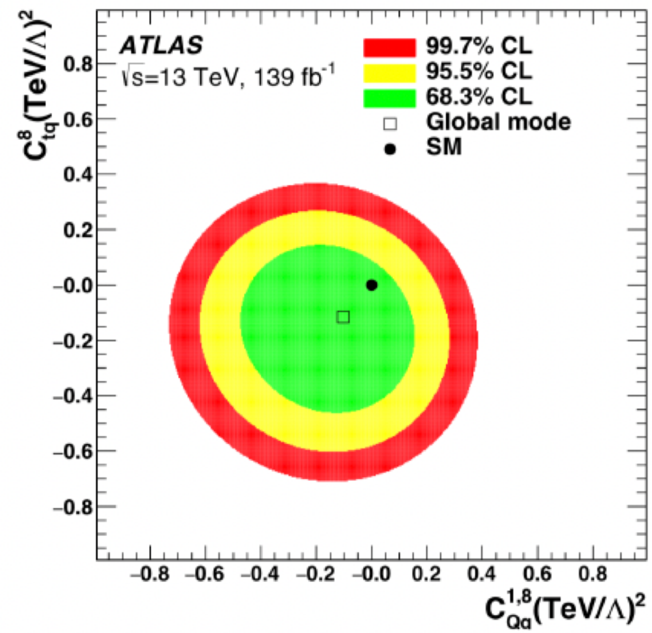

Differential $t\bar{t}$ cross-section measurements using boosted top quarks in the all-hadronic final state with 139 ifb of ATLAS data [arXiv:2205.02817]

New measurements, extending basis & HL-LHC projections

Process	Observable	$\sqrt{s}$	$\int \mathscr{L}$	Experiment
$pp \to t\bar{t}$	$d\sigma/dm_{t\bar{t}}$ (15+3 bins)	13 TeV	140 fb^{-1}	CMS
$pp \to t\bar{t}$	$dA_C/dm_{t\bar{t}}$ (4+2 bins)	13 TeV	140 fb^{-1}	ATLAS
$pp \to t\bar{t}Z$	$d\sigma/dp_T^Z$ (7 bins)	13 TeV	140 fb^{-1}	ATLAS
$pp \to t\bar{t}\gamma$	$d\sigma/dp_T^\gamma$ (11 bins)	13 TeV	140 fb^{-1}	ATLAS
$pp \to t\bar{t}H + tHq$	σ	13 TeV	140 fb^{-1}	ATLAS
$pp \to tZq$	σ	13 TeV	77.4 fb^{-1}	CMS
$pp \to t\gamma q$	σ	13 TeV	36 fb^{-1}	CMS
$pp \to t\bar{t}W$	σ	13 TeV	36 fb^{-1}	CMS
$pp \to t\bar{b}$ (s-ch)	σ	8 TeV	20 fb^{-1}	LHC
$pp \to tW$	σ	8 TeV	20 fb^{-1}	LHC
$pp \to tq$ (t-ch)	σ	8 TeV	20 fb^{-1}	LHC
$t \to Wb$	F_0, F_L	8 TeV	20 fb^{-1}	LHC
$p\bar{p} \to t\bar{b}$ (s-ch)	σ	1.96 TeV	9.7 fb^{-1}	Tevatron
$e^-e^+ \to b\bar{b}$	R_b , A_{FBLR}^{bb}	$\sim$ 91 GeV	202.1 pb^{-1}	LEP/SLD

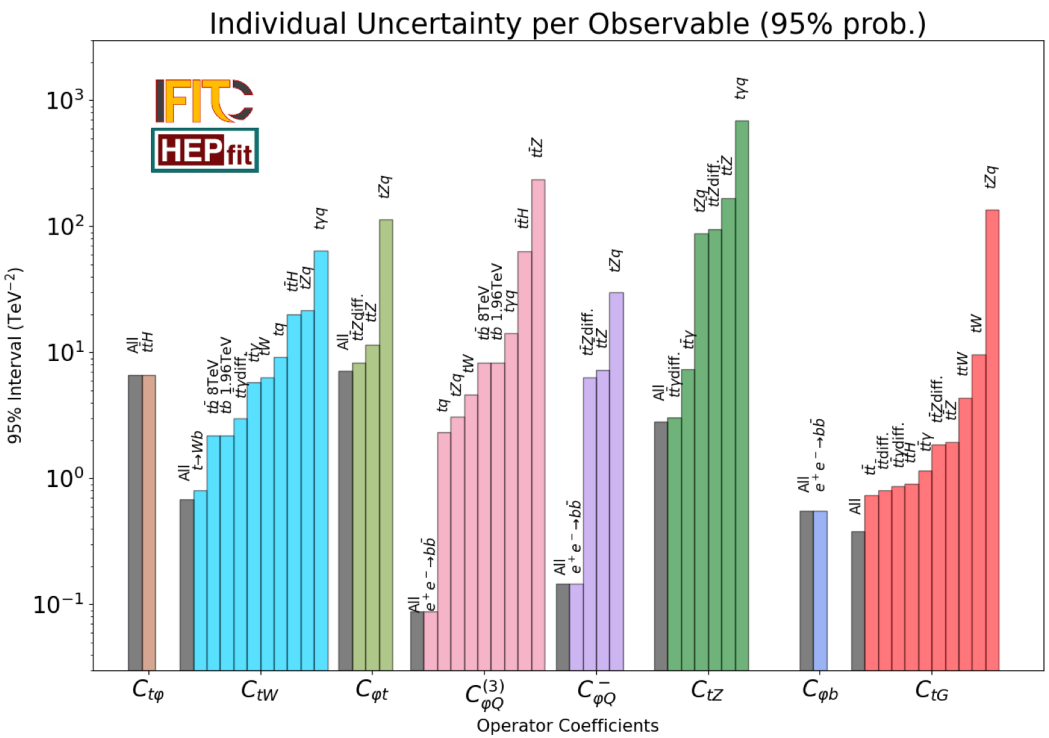

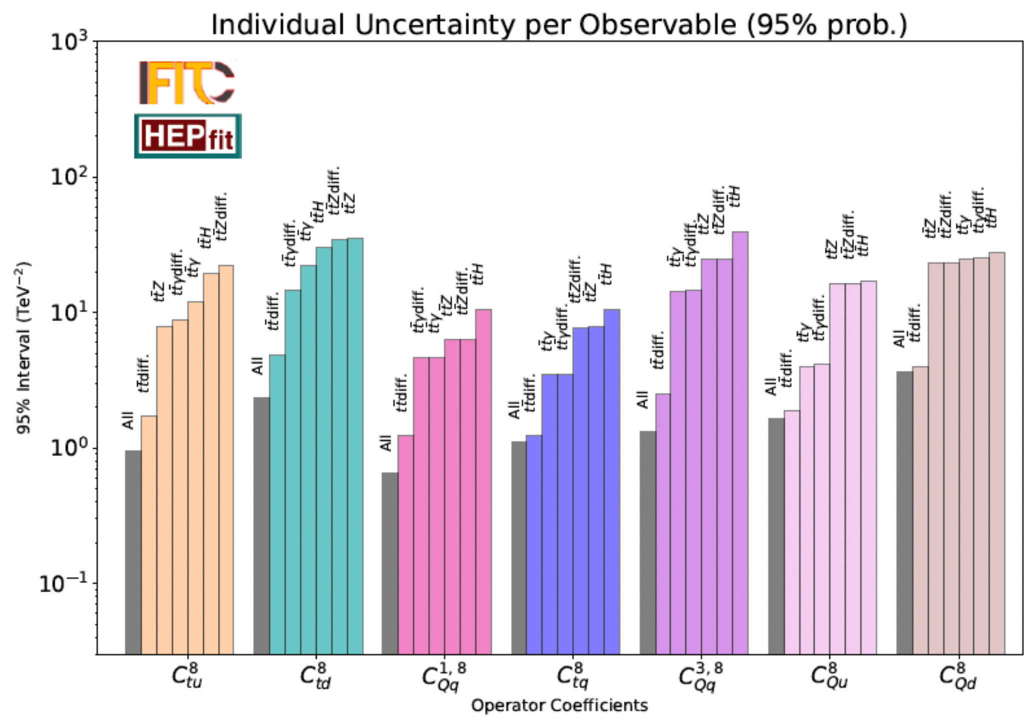

Prospects for future linear and circular e+e- colliders

- Including also QQll operators (besides the QQqq and 2F op.) in the global fit
- Only linear terms considered
- **Input observables in *e⁺e⁻ →bb*, *tt* and *ttH* production**
- **Full advantage of running at different CM energies (and even two beam polarisations)**
- **The higher-energy measurements are more relevant for the QQll operators**

Machine	$\mathrm{P}_{e^+}/\mathrm{P}_{e^-}$	Energy	Luminosity	Observables
ILC	$\pm 30\%/\mp 80\%$	250 GeV 500 GeV 1 TeV	2 ab^{-1} 4 ab^{-1} 8 ab^{-1}	$\sigma_{b\bar{b}}$, $A_{FB}^{b\bar{b}}$, $\mathcal{O}_{t\bar{t}}$, $\sigma_{t\bar{t}H}$
CLIC	$0\%/\pm 80\%$	380 GeV 1.5 TeV 3 TeV	1 ab^{-1} 2.5 ab^{-1} 5 ab^{-1}	$\sigma_{b\bar{b}}$, $A_{FB}^{b\bar{b}}$, $\mathcal{O}_{t\bar{t}}$, $\sigma_{t\bar{t}H}$
CEPC/FCC-*ee*	Unpolarised	Z-pole 240 GeV 350 GeV 360/365 GeV	57.5/150 ab^{-1} 20/5 ab^{-1} 0.2 ab^{-1} 1/1.5 ab^{-1}	$\sigma_{b\bar{b}}$, $A_{FB}^{b\bar{b}}$, $\mathcal{O}_{t\bar{t}}$

Inputs/Observables:
JHEP10(2018)168
arXiv: 2206.08326

Expected constraints for ILC

- ILC (>500 GeV) is ideal for EW couplings: improvements by factors of up to 200
- Two different energies above the *tt* threshold needed to constrain all 2F and 4F operators
- The two sets of operators have very different scaling with energy:
4F op. grows quadratically, while 2F op. dependence is constant or grows only linearly

arXiv: 2205.02140

Current and expected constraints

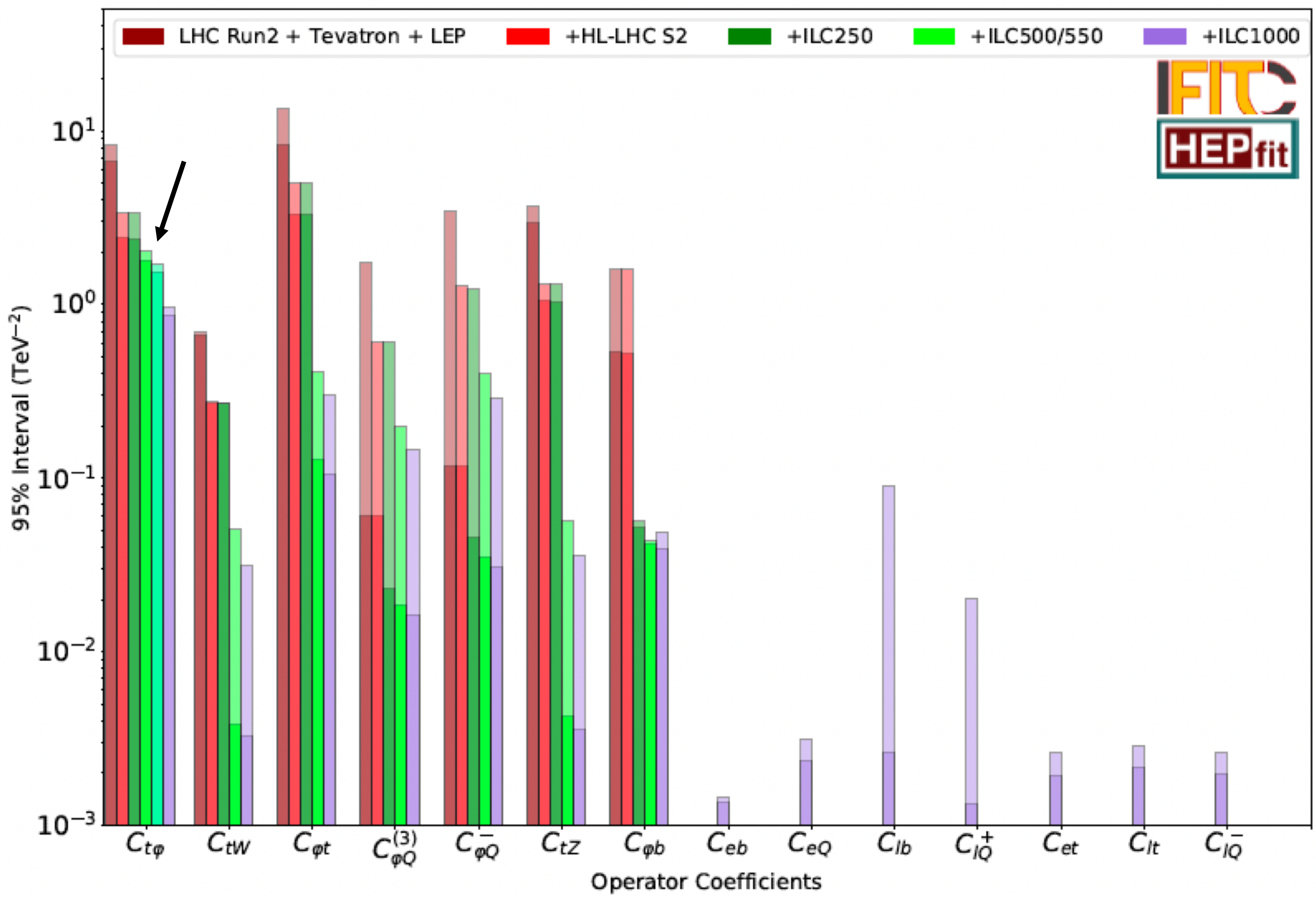

The global fit includes also QQqq operators and C_{tG}

Solid bars: individual fit
Shadowed bars: global fit

- Limits are significantly better at linear e^+e^- than circular e^+e^- not only because of higher collision energies but also polarized beams which help lift degeneracies

arXiv: 2205.02140

Current and expected constraints

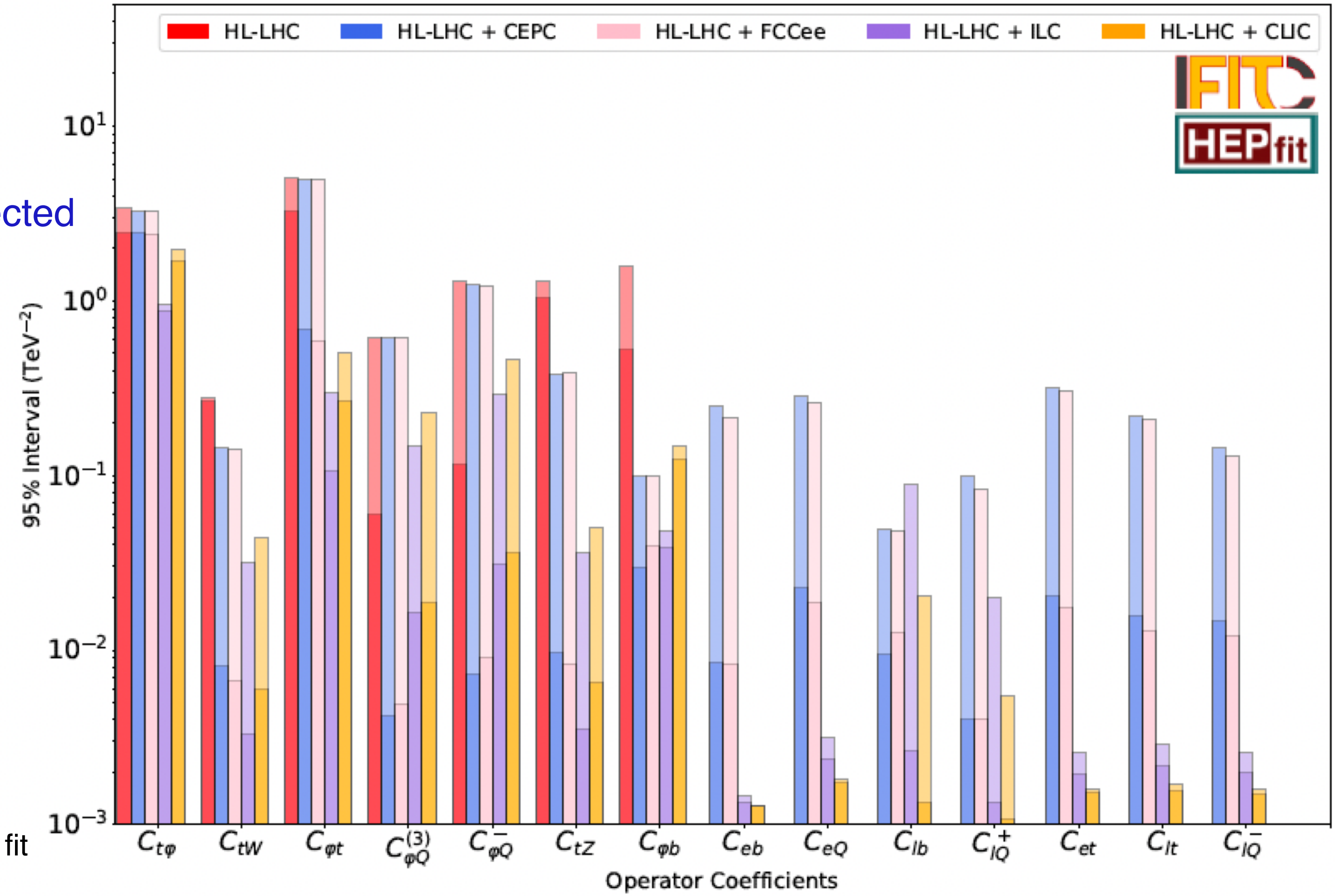

Solid bars: individual fit
Shadowed bars: global fit